

This work has been submitted to the KeAi for possible publication. Copyright may be transferred without notice, after which this version may no longer be accessible

arXiv:2512.12357v1 [cs.CV] 13 Dec 2025

TCLearf-Net: a transformer-convolution framework with global-local attention for robust in-field lesion-level plant leaf disease detection

Zishen Song^{a,1}, Yongjian Zhu^{b,1}, Dong Wang^{c,*}, Hongzhan Liu^{a,*}, Lingyu Jiang^d,
Yongxing Duan^c, Zehua Zhang^c, Sihan Li^c and Jiarui Li^c

^a*School of Optoelectronic Science and Engineering, South China Normal University, Guangzhou, 510006, Guangdong, China*

^b*College of Engineering Physics, Shenzhen Technology University, Shenzhen, 518118, Guangdong, China*

^c*Faculty of Intelligent Technology, Shanghai Institute of Technology, Shanghai, 201418, Shanghai, China*

^d*Graduate School of Information Sciences, Tohoku University, Sendai, 9808579, Miyagi, Japan*

ARTICLE INFO

Keywords:

Lesion-level disease detection
In-field detection
Transformer-convolution hybrid
Global-local attention
Daylily-Leaf datasets

ABSTRACT

Timely and accurate detection of foliar diseases is vital for safeguarding crop growth and reducing yield losses. Yet, in real-field conditions, cluttered backgrounds, domain shifts, and limited lesion-level datasets hinder robust modeling. To address these challenges, we release Daylily-Leaf, a paired lesion-level dataset comprising 1,746 RGB images and 7,839 lesions captured under both ideal and in-field conditions, and propose TCLearf-Net, a transformer-convolution hybrid detector optimized for real-field use. TCLearf-Net is designed to tackle three major challenges. To mitigate interference from complex backgrounds, the transformer-convolution module (TCM) couples global context with locality-preserving convolution to suppress non-leaf regions. To reduce information loss during downsampling, the raw-scale feature recalling and sampling (RSFRS) block combines bilinear resampling and convolution to preserve fine spatial detail. To handle variations in lesion scale and feature shifts, the deformable alignment block with FPN (DFPN) employs offset-based alignment and multi-receptive-field perception to strengthen multi-scale fusion. Experimental results show that on the in-field split of the Daylily-Leaf dataset, TCLearf-Net improves mAP@50 by 5.4 percentage points over the baseline model, reaching 78.2%, while reducing computation by 7.5 GFLOPs and GPU memory usage by 8.7%. Moreover, the model outperforms recent YOLO and RT-DETR series in both precision and recall, and demonstrates strong performance on the PlantDoc, Tomato-Leaf, and Rice-Leaf datasets, validating its robustness and generalizability to other plant disease detection scenarios.

1. Introduction

Agriculture is a cornerstone of the global economy, yet climate change and ecological degradation are elevating the incidence of foliar diseases, with consequent yield losses and economic damage (Ristaino et al., 2021). Leaf-borne pathogens reduce the photosynthetically active area, disrupt transpiration, and trigger systemic stress responses, so even small, early-stage lesions can translate into substantial yield penalties if

*Corresponding authors: dongwang@sit.edu.cn (D. Wang); lhzcnu@163.com (H. Liu).

¹These authors contributed equally to this work.

not treated promptly. Early warning therefore hinges on lesion-level monitoring, where individual spots are detected before they coalesce into whole-leaf infections.

Daylily cultivation, for example, has expanded rapidly in Yunzhou, China, generating 75,000-105,000 CNY per hectare and contributing significantly to poverty alleviation (Peng et al., 2024). However, abnormal temperature and humidity have increased the probability of disease outbreaks, eroding these gains (Wei et al., 2022). Reliable, in-field, lesion-level detection is thus essential for timely chemical or biological intervention and for sustaining the economic benefits of high-value crops such as daylily.

These challenges highlight the need for disease detection and intervention. Environmental sensors (e.g., temperature, humidity) monitor plant health at the macro level but cannot localize lesions and are sensitive to deployment conditions. In contrast, low-cost RGB cameras on GPS-enabled platforms provide flexible on-site lesion localization. This generates large volumes of images requiring an automated analysis method.

Traditional methods such as SVM, ANN, and decision trees rely on hand-crafted features with classifiers. However, these approaches are insufficiently robust under cluttered field conditions and domain shifts (Khan et al., 2024; Banerjee et al., 2023; Hossain et al., 2018; Joshi et al., 2022). In recent years, CNN-based models have replaced manual feature engineering and improved robustness to background interference (Farjon et al., 2023). They can learn hierarchical features directly from raw RGB images. Representative works include DGP-SNNet for fine-grained tomato disease discrimination (Tiancan et al., 2024), mixed-data augmentation for robust rice leaf classification (Haikal et al., 2024), an improved ResNet50 for mildew detection in grapevine (Sagar et al., 2025), the 28-layer DeepPlantNet (Ullah et al., 2023), and a ResNet50-MobileNetV2 ensemble for efficient tomato detection (Bharathi et al., 2025). These methods improved disease recognition accuracy through architectural improvements and data augmentation. However, the datasets used in these studies typically contain images in which the diseased leaf occupies a large portion of the image area and the background is either simple or only slightly complex. We refer to such datasets as ideal datasets. When these methods are applied to images captured under real-world conditions, where multiple leaves appear in a single frame and the background contains objects that visually resemble disease symptoms, which we refer to as in-field dataset, they often exhibit misclassification issues.

This limitation arises because convolutional models face constraints in receptive-field size and long-range context modeling (Zhang et al., 2020), which causes them to focus only on local regions such as specific lesions on leaves or background elements that visually resemble disease symptoms, while ignoring

the semantic relationships between the disease areas and the leaf, or between the leaf and the background. Although increasing the network depth can theoretically enlarge the receptive field, it often comes at the cost of reduced feature-map resolution, which may result in the loss of important object details. To further address this issue and enhance the receptive field, transformer-based architectures have been introduced to capture global semantic dependencies and improve robustness across multiple scales.

Transformer-based models have recently attracted attention in plant disease detection. For example, CAST-Net (Zhang et al., 2024b) combined convolution and self-attention for leaf disease recognition, MobileH-Transformer (Thai and Le, 2025) integrated convolutional downsampling with transformer layers to improve classification, and other models applied multi-head attention and depthwise separable convolution for potato disease classification (Zhang et al., 2024c). But these studies rarely explored why transformers enhance performance and why they have been evaluated mainly on ideal datasets.

The existing methods are trained on datasets such as PlantVillage, Turkey-PlantDataset, PlantDoc, and AES-CD9214. However, most of these datasets do not represent field complexity such as lighting variations, scale variations, occlusions, and background clutter (Attri et al., 2023; Ghazal et al., 2024). Field images often include noisy backgrounds and unstable illumination, which can degrade model performance (Liu et al., 2025). Therefore, most research lacks sufficient validation under in-field conditions, limiting their generalization.

Most studies focus on whole-leaf classification or diseased leaf detection (leaf-level detection), but overlook lesion-level localization and classification. This results in leaves being categorized as a single type, reducing classification precision. While a few studies collected field data, most did not release their datasets, further limiting reproducibility.

To sum up, we identify four major limitations:

1. Most studies use clean, ideal-conditions datasets; no high-quality public object detection dataset reflects in-field foliar disease conditions.
2. Existing works focus on leaf-level classification or detection, neglecting lesion-level objects with fine-grained annotation.
3. CNNs have a limited effective receptive field and weak long-range dependency modeling; simply deepening the network enlarges the theoretical field but reduces feature-map resolution and erodes

fine textures. By contrast, transformers incur quadratic attention complexity and exhibit weak spatial inductive bias, which can lead to diffuse attention under clutter and higher data requirements.

4. In-field scenarios, lesions vary in size, leading to intra-class feature inconsistency and complicating multi-scale fusion.

Limitations 1 and 2 have also been highlighted in recent reviews ([Bhargava et al., 2024](#); [Jafar et al., 2024](#); [Simhadri et al., 2024](#)). Once addressed, the next challenge is tackling limitations 3 and 4.

To address these challenges, it is necessary to construct a high-quality in-field dataset with lesion-level annotations. Models should be able to suppress background noise effectively. The limitations of convolutional models underscore the need for transformer-based architectures. Prior works ([Thai et al., 2023](#); [Reis and Turk, 2024](#); [Chakrabarty et al., 2024](#); [Huang et al., 2025](#)) have demonstrated that integrating convolution module with transformers can enhance plant disease classification. However, most of these studies employ single branch transformer architectures, which lead to large training data requirements. In addition, these models are primarily designed for ideal datasets; they either lack validation on in-field datasets or exhibit poor robustness when evaluated in real-world field conditions.

Multi-scale detection remains a significant challenge. Beyond the complications introduced by complex backgrounds, a major obstacle in in-field datasets is the variability in lesion scale. Techniques such as lateral feature fusion in feature pyramid networks (FPN) can enhance semantic richness, but they often suffer from feature misalignment, which impairs the detection of small lesions ([Huang et al., 2021](#); [Van Quyen and Kim, 2023](#)). The deformable convolutions employed in the feature alignment pyramid network (FaPN) ([Liu et al., 2023](#)) offer valuable inspiration, and we accordingly incorporate this strategy into our own framework.

To fill these research gaps, this study proposes TCLeaf-Net and publishes two datasets. TCLeaf-Net is a transformer-convolution hybrid model for detecting daylily leaf diseases in complex field conditions. It integrates a transformer-convolution module (TCM) that combines efficient attention (EA) for global semantics with convolutional layers for local texture and color, while reducing computational complexity.

Inspired by FaPN, we adopt its feature selector and, to provide richer contextual cues for the alignment block, design a multi-receptive-field perception (MRFP) module. These components constitute a deformable alignment block with FPN (DFPN) that mitigates feature misalignment in multi-scale fusion, while the detection head subsequently localizes lesion regions. The rationale for each component is detailed in Section 2.1.

In addition, two lesion-level datasets, Daylily-Leaf (ideal) and Daylily-Leaf (in-field), are constructed and released, both with fine-grained bounding box annotations. Although modest in scale and coarsely categorized, they enable accurate lesion localization and provide a practical basis for early-stage classification. The datasets are also transferable to other crops and disease types, offering a valuable foundation for future fine-grained recognition and cross-task adaptation.

The main contributions of this paper are as follows:

1. This study builds and publishes two high-quality datasets, Daylily-Leaf (in-field) and Daylily-Leaf (ideal), supporting object detection research under real-world (in-field) and laboratory (ideal) conditions.
2. To focus on lesion areas and suppress background noise, this study combines convolution and transformer mechanisms and proposes a detection framework. The results demonstrate that this mechanism is effective in inhibiting background noise.
3. This study proposes a deformable alignment block with FPN (DFPN) to filter and align multi-scale features for better fusion, and introduce a raw-scale feature recalling and sampling (RSFRS) module to boost early semantic recall.
4. We empirically demonstrate that TCM mitigates transformer diffuse attention in cluttered field backgrounds, as evidenced by ablations and Grad-CAM analyses.

2. Method

2.1. The architecture of TCLeaf-Net

TCLeaf-Net mainly consists of a transformer-convolution hybrid backbone (TC backbone) and a deformable feature-alignment pyramid network (DFPN), followed by a decoupled detection head. As shown in Fig. 1, the RGB image F_{in} is first fed into the TC backbone to produce multi-scale features F_3, F_4, F_7 , where TCM suppresses non-leaf background and mitigates the diffuse-attention tendency of pure transformers, and RSFRS adaptively combines bilinear and convolutional downsampling to retain pre-downsampling spatial detail. The features are then input to DFPN for offset-based alignment and multi-receptive-field fusion, yielding F_9, F_{10}, F_{11} . Finally, three scale-specific decoupled heads perform classification and bounding-box regression, and the final detections are obtained after confidence thresholding and non-maximum suppression (NMS). The following sections describe each part in detail.

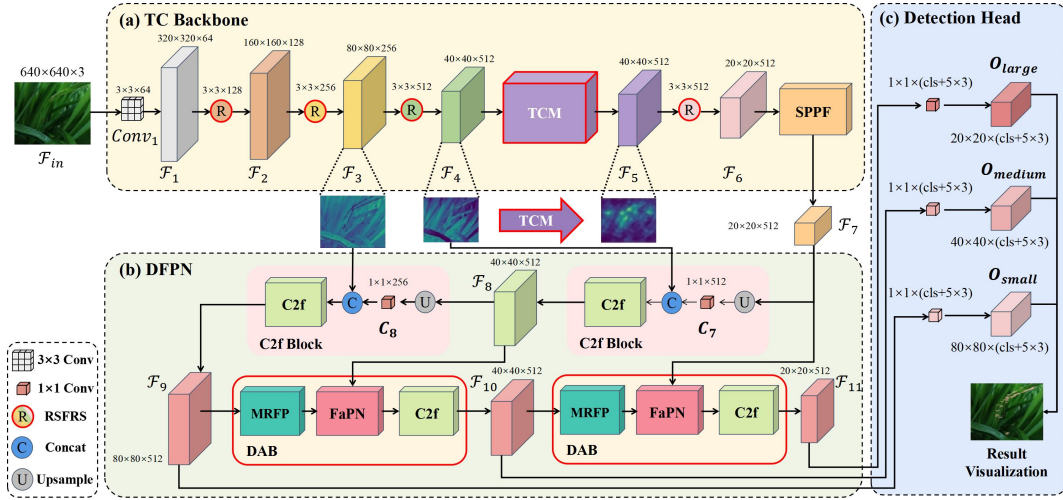


Fig. 1: Overall architecture of TCLeaf-Net. Modules proposed in this work are highlighted with bold red outlines.

2.2. TC backbone

Given an RGB image $F_{in} \in \mathbb{R}^{640 \times 640 \times 3}$, the backbone applies a small-step overlapping patch embedding (SSOPE) layer, a 3×3 convolution with stride 2, to downsample the input while maintaining local continuity, producing $F_1 \in \mathbb{R}^{320 \times 320 \times 64}$. A raw-scale feature recalling and sampling (RSFRS) module then carries out a second downsampling stage and intra-scale interaction via interpolation, yielding three resolutions: F_2 at 160×160 , F_3 at 80×80 , and F_4 at 40×40 . To encode both local context and long-range relations, F_4 is passed to a TCM, which outputs $F_5 \in \mathbb{R}^{40 \times 40 \times 512}$. RSFRS is then applied to downsample F_5 to $F_6 \in \mathbb{R}^{20 \times 20 \times 512}$, and a combination of SPPF further transforms F_6 into $F_7 \in \mathbb{R}^{20 \times 20 \times 512}$, which is particularly informative for large-object detection.

2.2.1. SSOPE and RSFRS

To address the limitations of standard non-overlapping patch embeddings, which weaken spatial continuity and blur object boundaries (Fig. 2(a)-(b)), we adopt a small-scale overlapping strategy. While OPE (Xu et al., 2024) uses a 20×20 kernel with stride 16 to mitigate this issue (Fig. 2(c)), its large receptive field risks merging foreground and background. Our SSOPE variant (Fig. 2(d)) instead employs a compact 3×3 kernel with stride 2 to better preserve local detail. To complement this, we propose RSFRS (Fig. 3(i)), which combines learnable downsampling and non-parametric bilinear sampling. Following ideas from FPN (Lin et al., 2017), RSFRS recalls high-resolution cues by fusing a 3×3 stride-2 convolution and

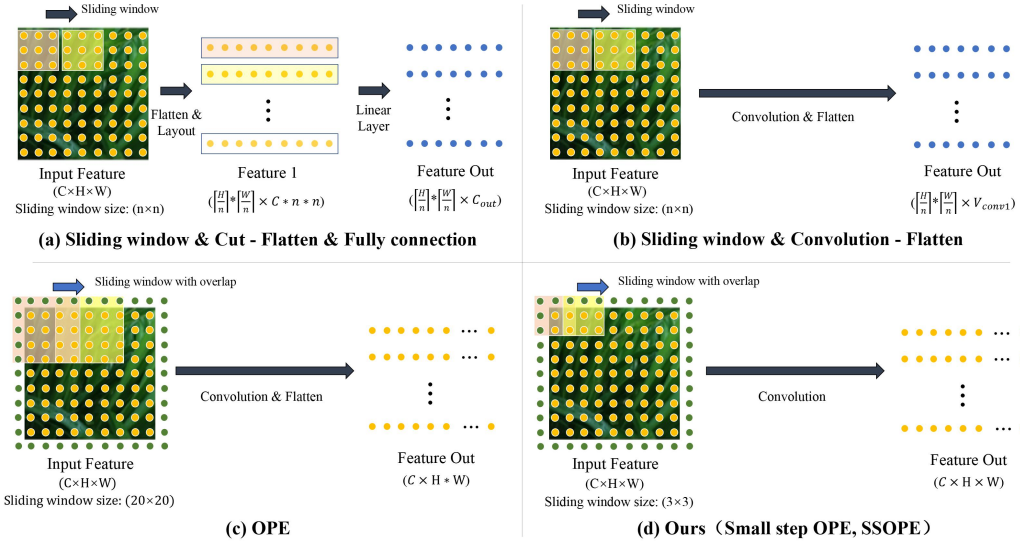


Fig. 2: Patch embedding strategies: standard, OPE, and the SSOPE.

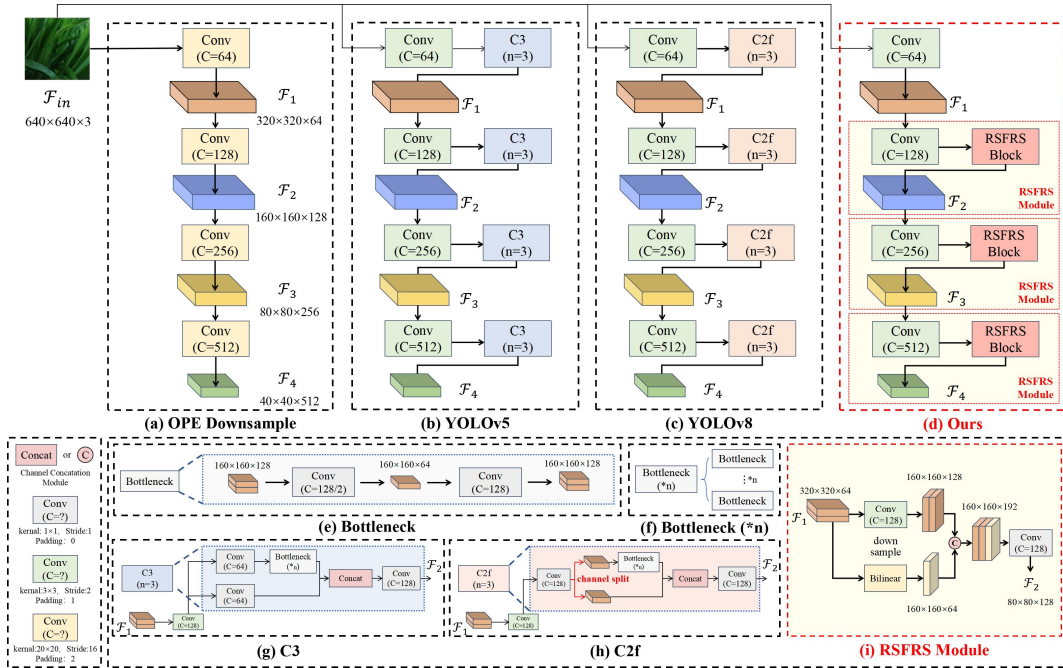


Fig. 3: Comparison of downsampling modules with various channel information fusion mechanisms.

bilinear interpolation via a 1×1 convolution:

$$V_2 = \text{Conv}_{3 \times 3}^{s=2}(V_1), \quad V_3 = \text{Bilinear}(V_1), \quad V_{\text{out}} = \text{Conv}_{1 \times 1}(\text{Concat}(V_2, V_3)). \quad (1)$$

Together, SSOPE and RSFRS enable compact yet expressive embeddings that retain fine-grained lesion details, inspired by both OPE and the Inception design (Szegedy et al., 2015).

2.2.2. TCM

Since disease symptoms primarily appear on leaf surfaces, effective lesion detection requires both local edge sensitivity and global contextual understanding. Convolutions excel at capturing high-frequency details such as leaf margins, but may mistake soil cracks or dead grass for lesions in complex field environments. In addition, scale shifts caused by varying leaf-camera distances can introduce false positives. In contrast, transformers provide a global receptive field and can model long-range spatial relationships (Goyal and Bengio, 2020); however, their weak inductive bias may lead to missing edge details under uneven illumination.

Most existing plant-disease detectors send convolutional features through a single CNN-to-transformer stream to capture global context (Thai and Le, 2025; Ji et al., 2021; Valanarasu et al., 2021). Yet vanilla transformers lack strong spatial inductive bias, so these pipelines converge slowly on small agricultural datasets and often miss subtle lesion cues (Zhang et al., 2025). We therefore introduce a parallel tri-branch transformer-convolution layer (TCL) that fuses CNN-style local attention (LAM) with transformer global attention (GAM) and a residual branch. Stacking four TCLs forms the TCM (Fig. 4), enabling simultaneous capture of fine-grained edges and long-range semantics.

Each TCL (Fig. 4(b)) comprises three parallel branches: a global-attention module (GAM, Fig. 4(c)), a local-attention module (LAM, Fig. 4(d)), and a residual branch (RB, Fig. 4(e)). Although this design alleviates the limitations of single branch self-attention models (Thai and Le, 2025), capturing both fine lesion details and global context in complex field environments remains challenging. The GAM employs EA (Choromanski et al., 2020) to model long-range dependencies, the LAM uses a convolution-batch-normalization-ReLU (CBR) block to highlight local structures, and the RB preserves the original input to stabilize training.

Given an input feature map $\mathcal{F}_4^{i,\text{in}}$, each TCL splits it into three branches. The LAM output V_1^i and GAM output V_2^i are concatenated and compressed via a 1×1 convolution, then reshaped and added to the residual branch output V_{res}^i to produce the final TCL output:

$$\mathcal{F}_4^{i,\text{out}} = \text{Reshape}(\text{Conv}_{1 \times 1}(\text{Concat}[V_1^i, V_2^i])) + V_{\text{res}}^i, \quad i = 1, 2, 3, 4. \quad (2)$$

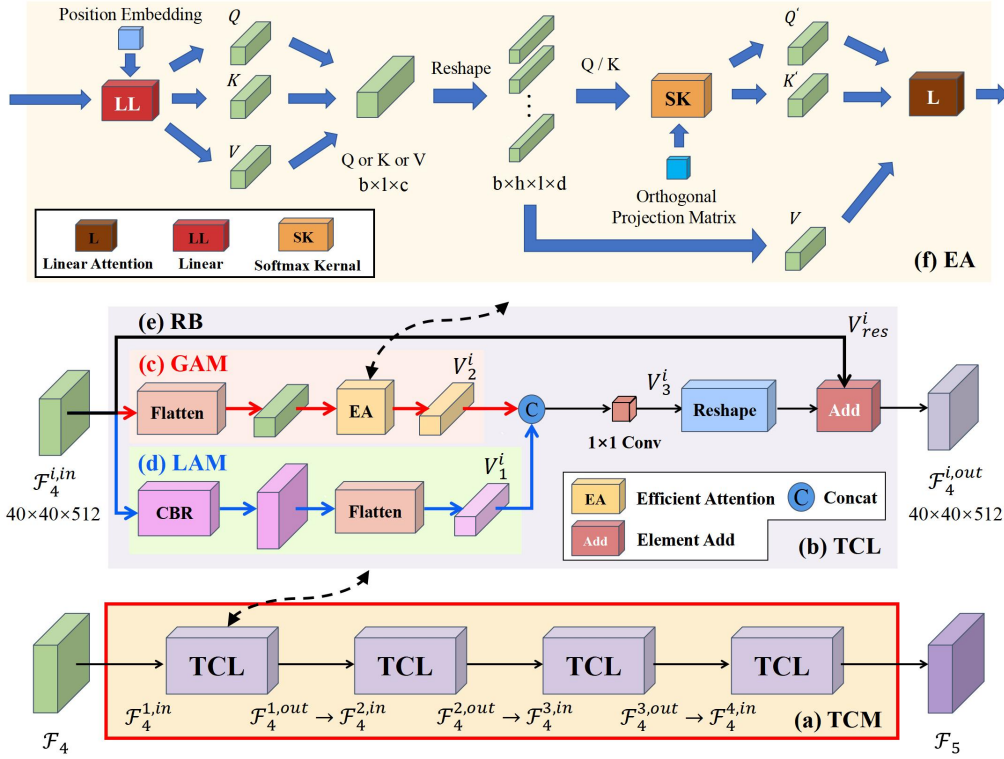


Fig. 4: Structures of the TCM (a) and TCL (b) modules.

Repeating this process across the four stacked TCLs progressively refines both local and global representations.

Efficient attention (EA): While transformers provide essential global modeling capacity for distinguishing leaves from lesions in complex agricultural scenes, their computational cost limits practical deployment. Standard multi-head self-attention (MHSA) has quadratic complexity $O(L^2d)$, where $L = H \times W$ denotes the number of tokens extracted from a feature map of height H and width W , and d is the channel (feature) dimension. This cost impedes real-time inference in resource-constrained scenarios.

To address this, we integrate EA within each TCL block. EA approximates softmax attention using randomized feature mappings, reducing complexity to linear $O(Lmd)$ ($m \ll L$) while preserving global dependencies. For an input of $8 \times 1600 \times 32$, standard MHSA requires $\sim 2.56 \times 10^9$ operations versus EA's 8.19×10^5 , a four-order magnitude reduction. The core EA workflow is as follows: random Gaussian matrices are sampled and processed by QR decomposition to obtain an orthogonal projection block $Q_{\text{block}} \in \mathbb{R}^{m \times d}$, which is then scaled to produce the final projection matrix $P = \Lambda Q_{\text{block}}$. Queries Q_i and keys K_j are mapped

to a random feature space using

$$\phi(x) = \exp\left(xP^\top - \frac{1}{2}\|x\|^2 - c_x\right), \quad (3)$$

where c_x stabilizes the computation for numerical stability.

2.2.3. DFPN with DAB

The conventional feature pyramid network (FPN) (Lin et al., 2017) (Fig. 5(b)) fuses semantic and spatial features through top-down pathways but suffers from semantic degradation and limited bottom-up information flow. PANet (Wang et al., 2019) addresses this with additional bottom-up paths to enhance fine-grained details. However, (Huang et al., 2021) shows that spatial misalignment during feature fusion, caused by downsampling, impairs localization and classification accuracy (Mingyue et al., 2022).

To resolve this, we propose a deformable alignment block (DAB) that integrates three modules: MRFP, FaPN, and C2f. As shown in Fig. 5, the original FPN is modified by replacing the red-boxed region in Fig. 5(c) with the proposed DAB (see Fig. 5(a)), resulting in the DFPN.

In the MRFP, parallel 5×5 and 7×7 depthwise separable convolutions (DWConv) are employed to substantially enlarge the receptive field and aggregate multi-scale context. Previous studies have shown that the multi-receptive-field design provided by parallel, multi-scale kernels can effectively improve object localization accuracy (Liu et al., 2018; Gao et al., 2019). Therefore, introducing these richer contextual features is intended to supply FaPN with more precise references for offset prediction, thereby enhancing the accuracy of the subsequent deformable alignment.

The architecture of DAB is detailed in Fig. 6(a). The upper-level feature $F_{9/10}$ first passes through the MRFP module (Fig. 6(b)), which applies 5×5 and 7×7 DWConv followed by a 1×1 convolution, expanding the receptive field with minimal parameter increase. The resulting feature $\hat{F}_{9/10}$ is concatenated with the corresponding lower-level feature $F_{8/7}$, and the combined tensor is fed into FaPN.

Within FaPN, the lower-level feature first enters the feature selection module (FSM), which computes channel-wise weights via global average pooling, a 1×1 convolution, and a sigmoid activation to produce an enhanced representation F_{arm} . Next, $\hat{F}_{9/10}$ is concatenated with F_{arm} and processed by a 1×1 convolution to generate the offset map F_{offset} . This map guides a deformable convolution (DConv) that produces the

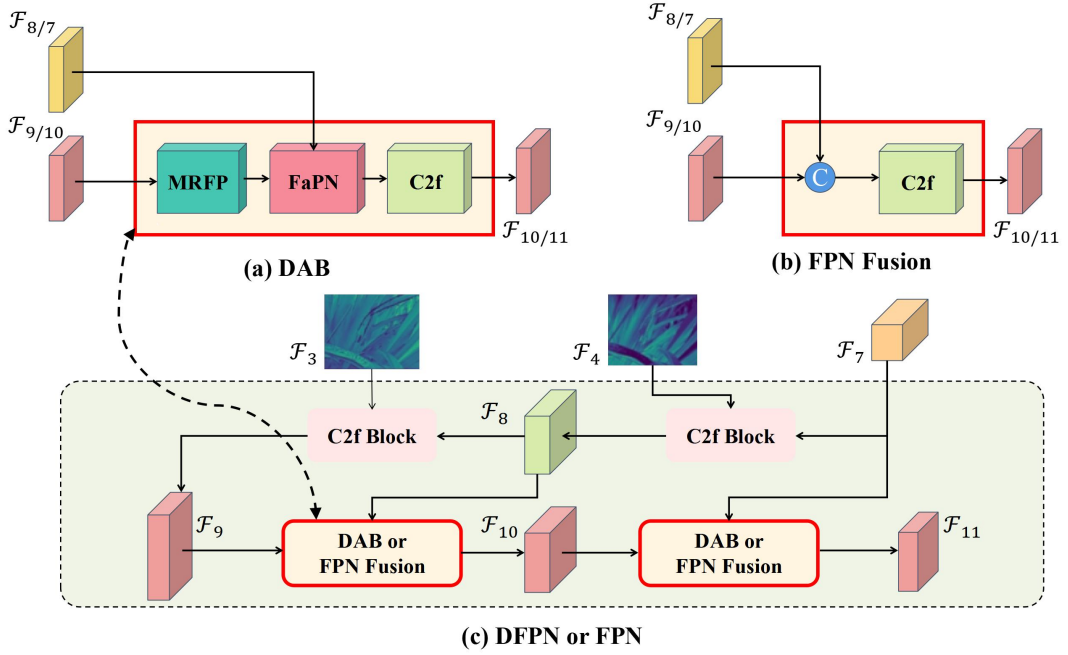


Fig. 5: Architectural comparison between the proposed DFPN and the conventional FPN.

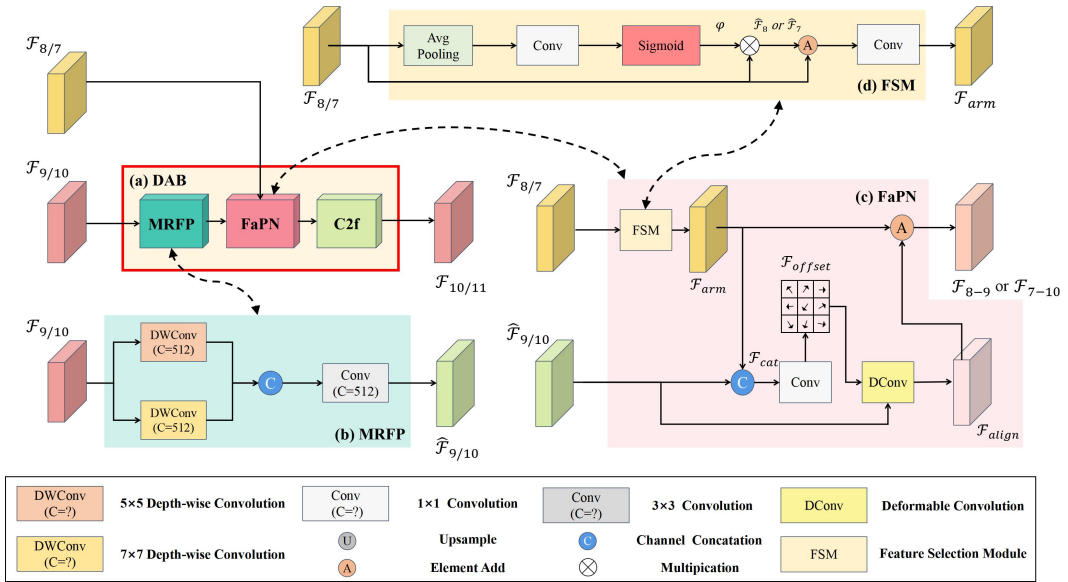


Fig. 6: Architecture of the deformable alignment block (DAB).

aligned feature F_{align} . The aligned feature and F_{arm} are then fused (by element-wise addition), and the result is refined by a C2f block to generate the output $F_{10/11}$.

2.3. Loss Function

The total loss includes three terms: CIoU-based box regression loss L_{box} for precise localization, Distribution Focal Loss L_{dfl} for coordinate refinement, and binary cross-entropy L_{cls} for objectness and classification. CIoU considers overlap, distance, and aspect ratio, leading to more accurate box predictions, and the final loss:

$$L_{\text{box}} = 1 - \text{CIoU}(b, b^*), \quad L_{\text{total}} = \lambda_{\text{box}} L_{\text{box}} + \lambda_{\text{dfl}} L_{\text{dfl}} + \lambda_{\text{cls}} L_{\text{cls}}. \quad (4)$$

2.4. Dataset construction

We introduce two publicly available daylily leaf disease detection datasets annotated solely at the lesion-level, comprising 1,746 images and 7,839 lesion instances, captured under both ideal and in-field conditions.

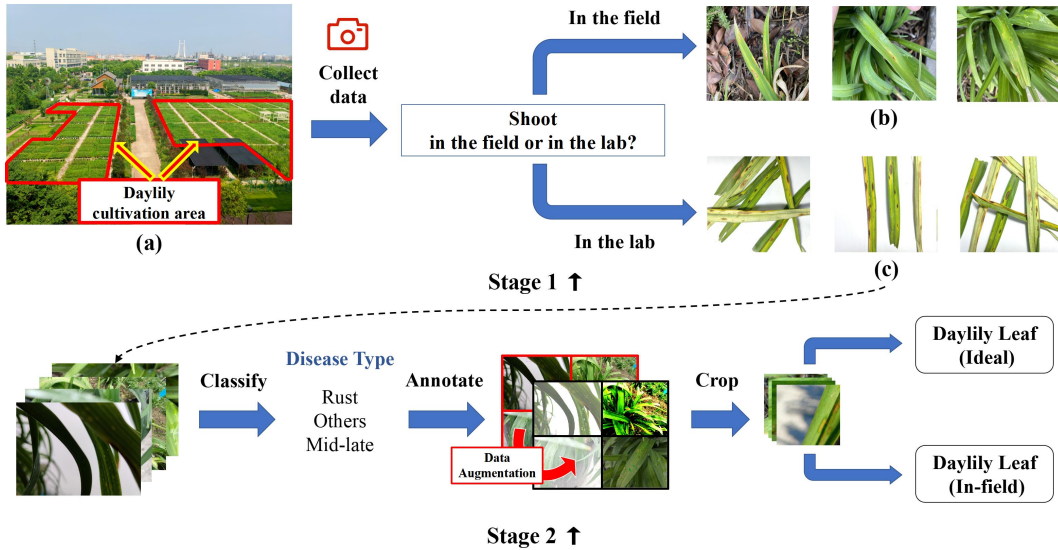


Fig. 7: Overview of dataset construction. Stage 1: data acquisition, including (a) garden location, (b) in-field image samples (in-field), and (c) laboratory image samples with white backgrounds (ideal). Stage 2: data processing workflow.

2.4.1. Data collection

Public leaf-image datasets are typically acquired in two settings: field (crop-canopy) and plain-background, each supporting either classification or detection tasks (Dong et al., 2022). Representative classification sets include PlantVillage, Turkey-PlantDataset, AES-CD9214, PlantDoc, FieldPlant, and Pigeon-pea, most of which target real-time disease detection in uncontrolled environments.

Most existing public datasets for detection show diseased leaves against simple backgrounds and often provide limited image quality. For instance, the Tomato-Leaf detection set (Kaggle), the Rice-Leaf set (Kaggle), and PlantDoc (Fig. 8(a)-(c)) mix field and controlled images into a single collection. The absence of high-quality, in-field data is now a major bottleneck in plant-disease detection.

To address this gap, we collected Daylily-Leaf images in Daylily cultivation area (Fig. 7(a)) in two scenarios: (i) in-field scenes (Fig. 7(b)) and (ii) a laboratory with a white background (Fig. 8(c)). Following the pipeline in Fig. 7 (stage 2), we performed expert annotation, data augmentation, and sliding-window cropping to accommodate the native 12-megapixel resolution. The final Daylily-Leaf dataset is divided into ideal (Fig. 7(d)) and in-field subsets (Fig. 8(e)), the former for controlled evaluation and the latter for realistic deployment tests.

Compared with the tomato, rice, and PlantDoc datasets (Fig. 8(a)-(c)), ours offers two advantages: (1) separate ideal and in-field subsets, enabling targeted evaluation, and (2) lesion-level (rather than leaf-level) annotations for precise localization and symptom classification.

2.4.2. Data processing

Using the protocol in (Dong et al., 2022), we manually annotated fine-grained lesion regions. As shown in Fig. 9, early-stage rust, leaf-spot, and powdery mildew are biologically distinct, but in some cases their visual characteristics may partially resemble each other. Moreover, due to varying real-world infection rates among disease types, the dataset exhibits inherent class imbalance. To mitigate both visual ambiguity and class imbalance, we regrouped the lesions into three broader categories, Rust, Others, and Mid-Late, based on morphological features and sample distribution. This coarse categorization simplifies the learning space and enhances model robustness in downstream detection. Although fine-grained disease labels are not the focus of this work, the current taxonomy could be extended in future studies using existing public classification datasets, enabling adaptation to more specific crop disease scenarios. All annotations were created using LabelImg, with representative examples shown in Fig. 10.

To improve model generalization, we applied extensive data augmentation including flips, rotations, brightness/contrast shifts, and simulated weather effects (e.g., clouds, snow), along with saturation changes, Gaussian blur, and mosaic overlays. After processing, the Daylily-Leaf (ideal) and Daylily-Leaf (in-field) datasets jointly comprise 1,746 images and 7,839 annotated lesion instances (Table 1), each subset further divided into training and validation sets.

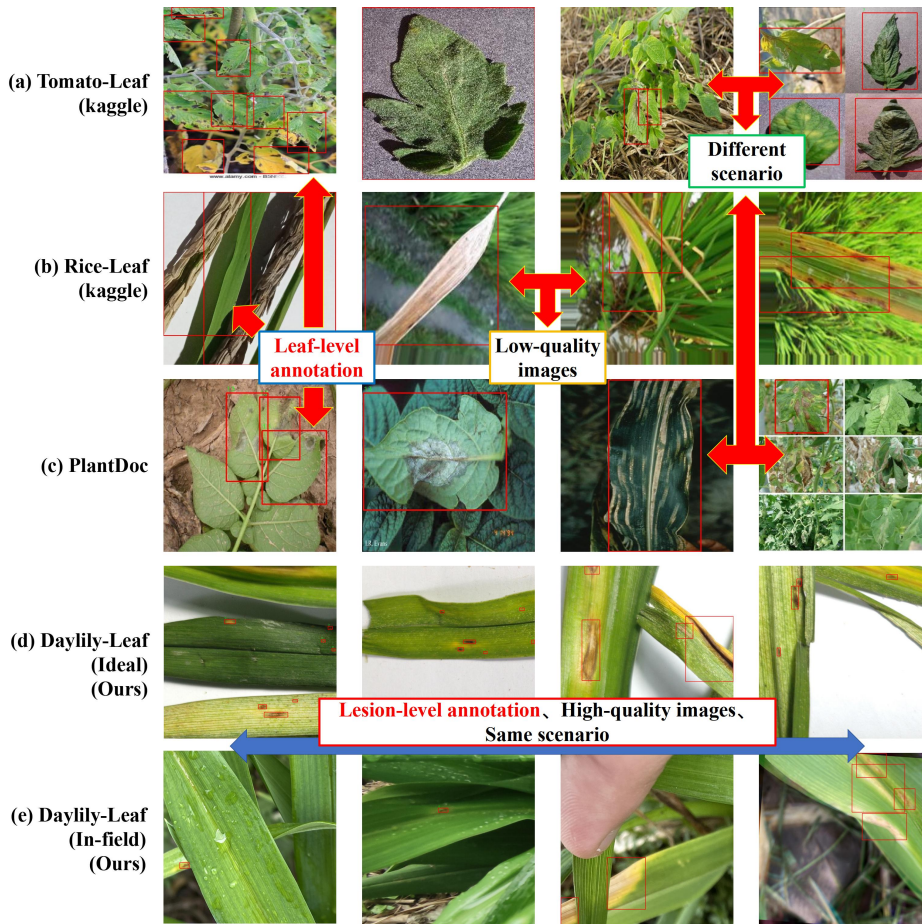


Fig. 8: Comparison of datasets with manually annotated ground-truth bounding boxes (shown in red).

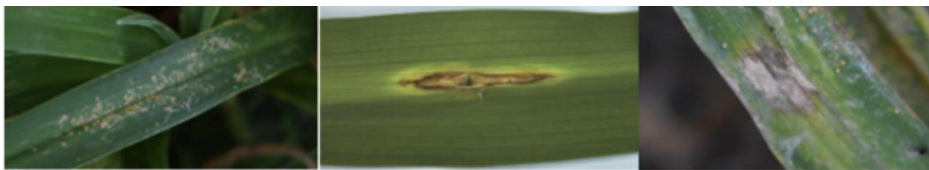


Fig. 9: Biological characteristics of three major categories of plant diseases.

3. Experiments and results

To benchmark our approach, we compare TCLeaf-Net against 13 mainstream object detectors, covering both convolution-based and transformer-based paradigms. The convolution-based baselines include YOLOv3 (Redmon and Farhadi, 2018), YOLOv5L (Jocher and Team, 2020), YOLOv6L (Li et al., 2022a), YOLOv8L (Team, 2023), YOLOv9C (Zhang et al., 2024a), YOLOv10L (Wang et al., 2024), and YOLO11L (Lee et al., 2024). In addition, we include six single branch transformer-based detectors:

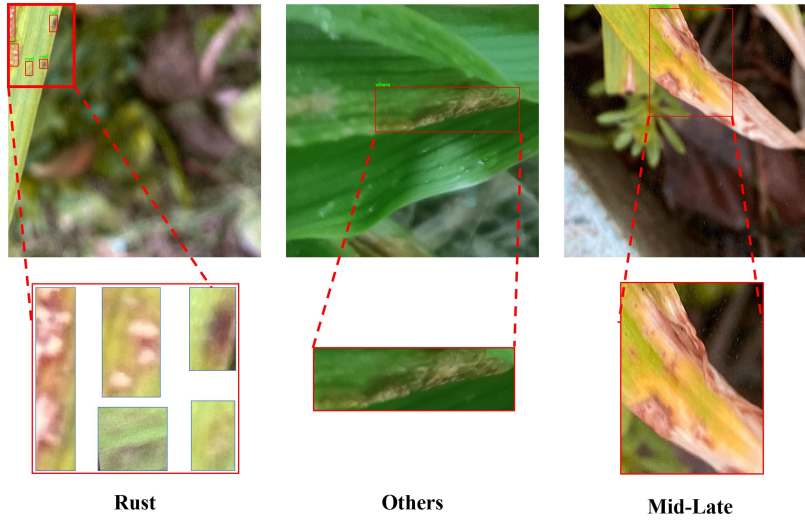


Fig. 10: The three disease types defined in this study.

Table 1

Statistics of the Daylily-Leaf (ideal and in-field) datasets.

Dataset	Subset	Img.	Tot.	R.	O.	M.L.
Ideal	Train	569	3877	2229	1228	420
	Val	244	1295	791	375	129
In-field	Train	653	1788	1169	552	67
	Val	280	879	469	374	36

Note. **Img.** = Number of images; **Tot.** = Total annotated lesions; **R./O./M.L.** = Numbers of rust, “others”-type, and mid-late stage lesions, respectively.

RTDETR-R50, RTDETR-R101, RTDETR-L, and RTDETR-X (Zhao et al., 2023), as well as the recently released YOLO12L and YOLO12X (Tian et al., 2025). All models trained from scratch and they are evaluated on both the Daylily-Leaf (ideal) and Daylily-Leaf (in-field) datasets constructed in this work, enabling a direct comparison of detection performance under controlled versus real-world agricultural conditions. Each experiment is run three times and averaged.

3.1. Experimental setting and metrics

During training, we employed the SGD optimizer with initial learning rate was set to 0.001 with a momentum of 0.937. The input images were resized to 640×640 pixels, and trained for 200 epochs with a batch size of 16. The detailed configuration of the experimental environment is summarized in Table 2.

Table 2

Experimental environment.

Type	Value
Operating system	Ubuntu 22.04 LTS
GPU	NVIDIA RTX 4090D (24 GB)
CPU	Intel Xeon Platinum 8481C
Software stack	Python 3.12, PyTorch 2.5.1, CUDA 12.4

Model quality and efficiency are reported with the following metrics: precision (P), recall (R), F1-score ($F1$), mean average precision at 0.50 IoU (mAP@50), mean average precision from 0.50 to 0.95 IoU (mAP@50:95), parameter count (Param.), and giga floating-point operations per inference (GFLOPs).

$$P = \frac{TP}{TP + FP}, \quad R = \frac{TP}{TP + FN}, \quad F1 = 2 \times \frac{P \times R}{P + R}. \quad (5)$$

Higher P , R , $F1$, mAP@50, and mAP@50:95 indicate better detection performance, whereas lower Param. and GFLOPs imply a lighter and faster model. In the following tables, \uparrow indicates that higher values are better, while \downarrow indicates that lower values are better.

3.2. Ablation experiment

Table 3 summarizes the ablation results. The base model YOLOv8L (Exp. 1) attains 87.8% and 72.8% mAP@50 on the ideal and in-field datasets, respectively. Introducing the TCM (Exp. 2) significantly improves precision, mAP@50, and mAP@50:95. Although recall decreases moderately, the overall F1 still increases, while also trimming the network from 43.6 M to 38.2 M parameters and reducing GFLOPs from 165.4 to 133.8.

Adding the RSFRS block (Exp. 3) increase recall on both datasets. However, precision decreases moderately on the ideal dataset, resulting in a slight dip in mAP@50 and leaving F1 almost unchanged.

Combining TCM with RSFRS (Exp. 5) or with DFPN (Exp. 6) delivers further improvements and a better balance between precision and recall.

The full model, TCM-Net (Exp. 7), integrates TCM, RSFRS and DFPN, achieving the best results: 89.5%/65.2% mAP@50/mAP@50:95 on the ideal dataset and 78.2%/55.1% on the in-field dataset. Compared with the baseline, this represents gains of +1.7 pp (ideal) and +5.4 pp (in-field) in mAP@50, while reducing computational cost by 7.5 GFLOPs and saved 8.7% GPU memory during training related to the base model.

Table 3

Ablation study of each proposed components on the Daylily-Leaf (ideal and in-field) datasets.

Exp.	Model	Ideal dataset					In-field dataset					GFLOPs ↓	Param. (M) ↓
		P (%) ↑	R (%) ↑	mAP@50 (%) ↑	mAP@50:95 (%) ↑	F1 (%) ↑	P (%) ↑	R (%) ↑	mAP@50 (%) ↑	mAP@50:95 (%) ↑	F1 (%) ↑		
1	Base	82.6	83.5	87.8	63.1	83.0	82.4	65.9	72.8	50.6	73.2	165.4	43.6
2	Base+TCM	86.9	81.1	88.4	64.0	83.9	88.8	63.3	75.4	54.0	73.9	133.8	38.2
3	Base+RSFRS	81.6	83.6	87.5	63.1	82.6	82.5	67.5	74.1	52.2	74.3	173.8	46.3
4	Base+DFPN	85.3	81.2	88.7	63.3	83.2	81.3	65.6	73.4	51.0	72.6	180.2	48.1
5	Base+TCM+RSFRS	86.5	81.7	88.9	64.9	84.0	85.8	65.4	75.9	53.6	74.2	142.7	41.9
6	Base+TCM+DFPN	85.2	82.8	89.1	65.0	84.0	85.8	66.8	76.0	53.0	75.1	149.0	42.4
7	Base+TCM+RSFRS+DFPN (Ours)	85.9	83.6	89.5	65.2	84.7	87.2	69.9	78.2	55.1	77.6	157.9	46.1
–	<i>Gain (Ours vs. Base model)</i>	+3.3	+0.1	+1.7	+2.1	+1.7	+4.8	+4.0	+5.4	+4.5	+4.4	-7.5	+2.5

Note. **Bold numbers** indicate the best results; **Base** = Base model; **Exp.** = Experiment; **Param.** = Parameters.

Table 4

Ablation results of SSOPE and RSFRS on the Daylily-Leaf (in-field) subset.

Exp.	Type	P (%) ↑	R (%) ↑	mAP@50 (%) ↑	mAP@50:95 (%) ↑
1	PTE	84.9	63.8	75.4	52.8
2	OPE (16×16)	85.5	66.2	76.8	53.6
3	SSOPE (3×3)	85.3	66.7	77.1	54.9
4	SSOPE (5×5)	84.3	64.9	75.5	52.8
5	SSOPE (7×7)	82.8	65.1	75.8	53.1
6	RSFRS (With SSOPE, ours)	87.2	69.9	78.2	55.1

Note. **PTE** = patch tokenizer with a 16×16 kernel; **OPE** = overlapping patch embedding; **SSOPE** ($n \times n$) = small-step OPE with $n \times n$ kernel.

These results demonstrate the complementary nature of the proposed modules and their effectiveness in improving detection accuracy, robustness and efficiency. Next, we further investigate the effects of individual components, beginning with detailed ablation studies on the RSFRS, SSOPE, and DFPN modules.

3.2.1. Ablation study on RSFRS and SSOPE

Table 4 compares six patch-embedding strategies on the Daylily-Leaf (ideal and in-field) subsets. The non-overlapping patch embedding (PTE) with a 16×16 window achieves only 75.4% and 52.8% in mAP@50 and mAP@50:95, with a recall of 63.8%. This supports earlier reports that large, gapless patches blur edges and hinder localization (Touvron et al., 2022).

Introducing an overlapping patch embedding (OPE, 16 × 16 kernel) elevates every evaluation metric, indicating that moderate redundancy helps retain boundary cues. When the kernel is reduced to the small stride OPE (SSOPE, 3 × 3), mAP@50 increases to 77.1% and mAP@50:95 to 54.9%, which corroborates reports that finer patches improve accuracy (Shu and Bain, 2024). Conversely, enlarging the kernel to 5 × 5 or 7 × 7 decreases precision and recall because the broader receptive fields over-smooth small lesions, illustrating the diminishing returns of excessively large kernels (Li et al., 2025).

Combining SSOPE (3×3) with the RSFRS block lifts precision and recall to 87.2% and 69.9%, indicating that RSFRS parallel resampling recovers early information loss without increasing false positives.

Table 5

Ablation results of the DFPN module on the Daylily-Leaf (in-field) dataset.

Type	P (%)↑	R (%)↑	mAP@50 (%)↑	mAP@50:95 (%)↑
FPN	85.8	65.4	75.9	53.6
BiFPN	82.5	68.6	75.9	53.1
PANet	79.1	67.4	76.3	54.1
DFPN (Ours)	87.2	69.9	78.2	55.1

Table 6

Comparison of model performance on Daylily-Leaf (ideal and in-field) datasets.

Model	Ideal dataset				In-field dataset				GFLOPs ↓	Param. (M) ↓
	P (%)↑	R (%)↑	mAP@50 (%)↑	mAP@50:95 (%)↑	P (%)↑	R (%)↑	mAP@50 (%)↑	mAP@50:95 (%)↑		
Convolution-based model										
YOLOv3	84.8	82.3	<u>88.3</u>	64.2	78.5	<u>68.1</u>	<u>74.2</u>	<u>52.6</u>	282.2	103.7
YOLOv5L	80.7	82.4	86.8	64.1	80.9	64.3	70.0	47.9	134.7	53.1
YOLOv6L	81.8	75.9	84.1	57.4	37.3	34.4	27.8	14.1	391.2	110.9
YOLOv8L	82.6	<u>83.5</u>	87.8	<u>63.1</u>	<u>82.4</u>	65.9	72.8	50.6	164.8	43.6
YOLOv9C	<u>85.7</u>	79.4	87.5	61.2	80.8	63.0	72.1	48.9	102.3	25.3
YOLOv10L	73.5	68.1	76.1	58.1	58.5	49.8	53.5	34.5	126.3	25.7
YOLO11L	80.2	76.9	84.9	58.1	66.2	58.6	63.4	40.3	<u>86.6</u>	25.3
Single branch transformer-based model										
RTDETR-L	63.0	62.4	61.9	39.1	53.5	49.0	47.7	28.7	108.0	32.8
RTDETR-X	55.6	56.0	54.1	33.1	43.8	48.5	38.9	23.0	232.4	67.3
RTDETR-R50	67.1	67.0	67.6	43.0	57.8	53.4	52.6	32.6	130.5	42.8
RTDETR-R101	63.2	65.1	65.4	42.3	58.2	52.7	52.6	33.1	191.4	61.8
YOLO12X	81.6	81.5	86.4	60.9	75.0	62.7	69.2	46.3	199.9	59.1
YOLO12L	81.6	78.4	84.8	58.3	80.5	59.7	68.7	45.2	89.4	26.4
Transformer-convolution hybrid model										
TCLeaf-Net (ours)	85.9	83.6	89.5	65.2	87.2	69.9	78.2	55.1	157.9	46.1
<i>Gain (Ours vs. 2nd best)</i>	+0.2	+0.1	+1.2	+1.0	+4.8	+1.8	+4.0	+2.5	-	-

Note. **Bold numbers** indicate the best result; underlining marks the second (2nd) best; **OOM** = out-of-memory error (GPU).

3.2.2. Ablation study on DFPN

Table 5 compares three necks on the in-field dataset. BiFPN yields 82.5% precision, 68.6% recall, and 75.9% mAP@50. PANet produces 79.1% precision, 67.4% recall, 76.3 percent mAP@50, and 54.1 percent mAP@50:95. DFPN attains the best result. These results show that DFPN offers the most balanced performance among the three designs under identical training settings.

3.3. Comparative experiment

Table 6 compares eight detectors on the Daylily-Leaf (ideal) and Daylily-Leaf (in-field) sets using mAP@50, mAP@50:95, precision and recall, while the training curves appear in Fig. 11.

As Fig. 11(a)-(b) show, most of the models reach at least 60% mAP@50 when trained and validated on the ideal dataset. When trained on the in-field dataset, however, their validation scores drop; YOLOv6L, YOLOv10L, YOLO11L and YOLO12X decline the most, revealing limited robustness to complex backgrounds, whereas the remaining models remain relatively stable.

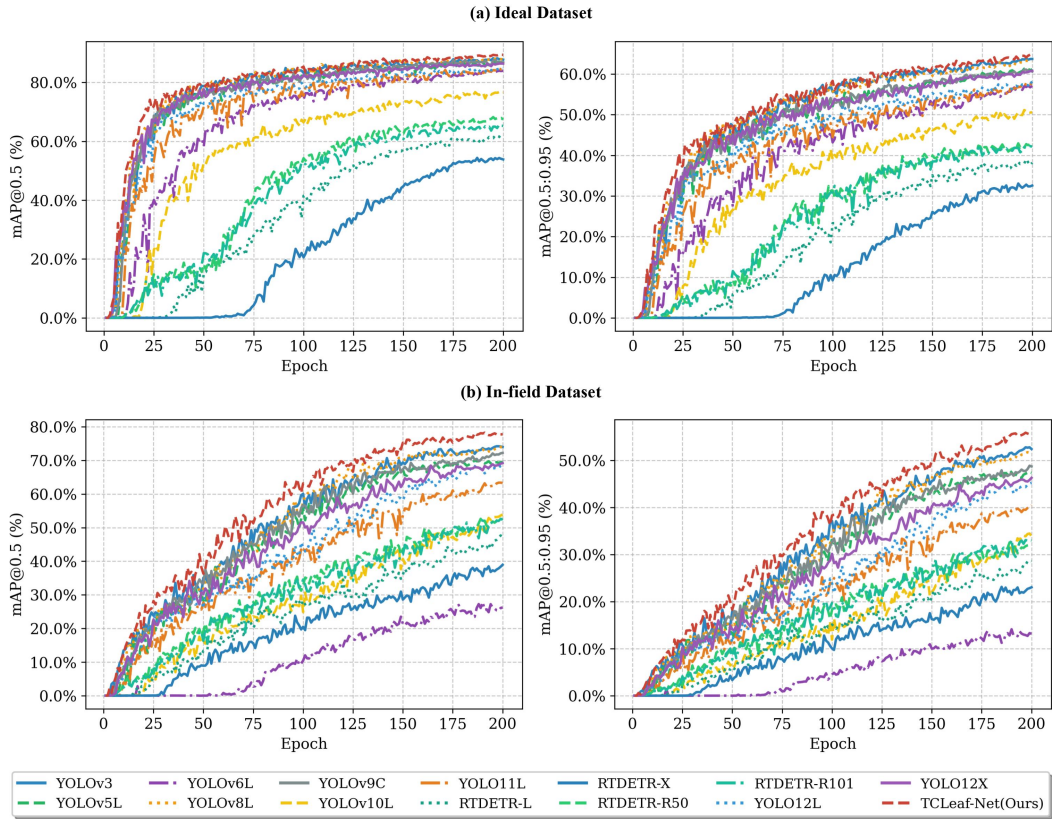


Fig. 11: Comparative experiments of TCLeaf-Net and other models (epoch-mAP@50 curves): (a) trained on the Daylily-Leaf (in-field) dataset; (b) trained on the Daylily-Leaf (ideal) dataset.

TCLeaf-Net delivers the best overall performance on the in-field dataset. Although YOLOv3 ranks second-best overall performance, it requires approximately $1.79\times$ more computation (GFLOPs) and $2.25\times$ more parameters than TCLeaf-Net. These efficiency gains stem from the TC backbone (Table 3, Exp. 2 and 5), whose TCM and RSFRS modules shorten the depth and reduce use of C2f blocks, cutting approximately GFLOPs by 13.7% and parameters by 3.9% relative to the base model YOLOv8L. By combining long-range spatial modeling with local feature attention, the TC backbone better captures relationships among leaves, lesions and background, which in turn lifts both precision and recall. On the ideal dataset, TCLeaf-Net also generalizes well, attaining 89.5% mAP@50, 65.2% mAP@50:95, 85.9% precision and 83.6% recall, again topping every competitor.

To gauge robustness, we computed the drop from the ideal to the in-field dataset across four metrics for each detector:

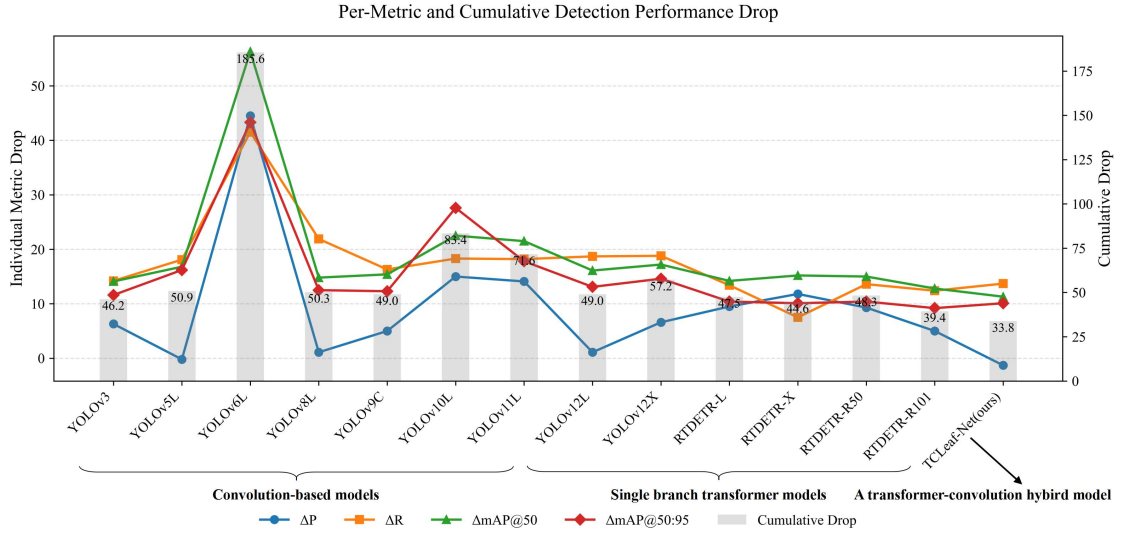


Fig. 12: Performance drop from Daylily-Leaf (ideal) to (in-field); values are in percentages (lower is better).

To gauge model robustness, we quantified the performance drop from the ideal to the in-field dataset across four key metrics—precision (ΔP), recall (ΔR), mAP@50 ($\Delta mAP@50$), and mAP@50:95 ($\Delta mAP@50:95$), for each detector:

$$\Delta \text{Metric} = \text{Metric}_{\text{ideal}} - \text{Metric}_{\text{in-field}}. \quad (6)$$

We summed these metric differences to calculate an overall sensitivity measure (cumulative performance drop). As shown in Fig. 12, TCLLeaf-Net achieves the smallest cumulative performance drop (33.8 percentage points, pp), indicating superior robustness to variations in background complexity. RTDETR-R101 follows closely with a cumulative drop of 39.4 pp, while YOLO-series models generally exhibit higher sensitivity (ranging from 46.2 to 83.4 pp). Notably, YOLOv6L shows the greatest performance degradation (185.6 pp), highlighting its vulnerability to challenging in-field conditions.

Interestingly, TCLLeaf-Net demonstrates a negative precision drop ($\Delta P = -1.3$ pp), suggesting improved precision in real-world scenarios, but the recall dropped. RT-DETR variants consistently exhibit moderate drops in recall but maintain relatively stable mAP scores, reflecting balanced robustness. In contrast, most YOLO models display larger and less consistent performance reductions across all metrics. Overall, TCLLeaf-Net provides the best trade-off among all models, underscoring its stability and reliability in complex, practical agricultural environments.

To provide qualitative insights into how TCGLeaf-Net achieves improved performance, we visualize representative detection scenarios from the in-field validation set.

3.4. Visualization

For a qualitative assessment under real-world conditions, six representative scenarios from the in-field validation set were chosen (Fig. 13(a)-(f)), illustrating the following challenges: (a) well-lit with leaves and background each occupying half the frame, (b) well-lit with multiple leaves, (c) low light with dense foliage and subtle, small lesions, (d) low light with multiple leaves and de-focused lesion areas, (e) well-lit, leaf-dominated scenes containing small lesion targets, and (f) well-lit with multiple leaves.

Fig. 13 presents a side-by-side comparison of the ground truth (GT; left), defined as images with human annotations, the output of the base model (middle), and that of TCGLeaf-Net (right). False positives in the model predictions are circled in white, and missed lesions are labeled as “missing”.

In detail, (a) the base model missed a partially occluded rust lesion; (b) and (c) exhibited confusion between lesion and non-lesion regions, resulting in missed detections; (d) defocused areas caused detection failure for the base model; (e) the base model failed to detect two small lesions, while TCGLeaf-Net missed only one; and (f) TCGLeaf-Net identified a lesion absent from the ground truth that the base model also failed to detect.

These examples show that TCGLeaf-Net demonstrates greater stability in the presence of complex backgrounds and blurring. While TCGLeaf-Net shows superior performance on our own Daylily-Leaf datasets, it is essential to confirm whether these improvements generalize to broader scenarios. Thus, we evaluate our model on three external, publicly available datasets.

3.5. Generalization experiments

To assess the generalization of TCGLeaf-Net beyond Daylily-Leaf datasets, we evaluated its performance against multiple YOLO and RT-DETR baselines on three widely used public leaf-disease detection datasets: PlantDoc, Tomato-Leaf, and Rice-Leaf, which represent varying degrees of scene complexity and image quality.

PlantDoc. PlantDoc comprises in-field images characterized by complex backgrounds and notable class imbalance. As reported in Table 7, TCGLeaf-Net achieves the highest mAP@50 (65.7%) and mAP@50:95 (52.5%), outperforming the strongest baseline (YOLO12X) by 2.1 and 2.7 percentage points, respectively.

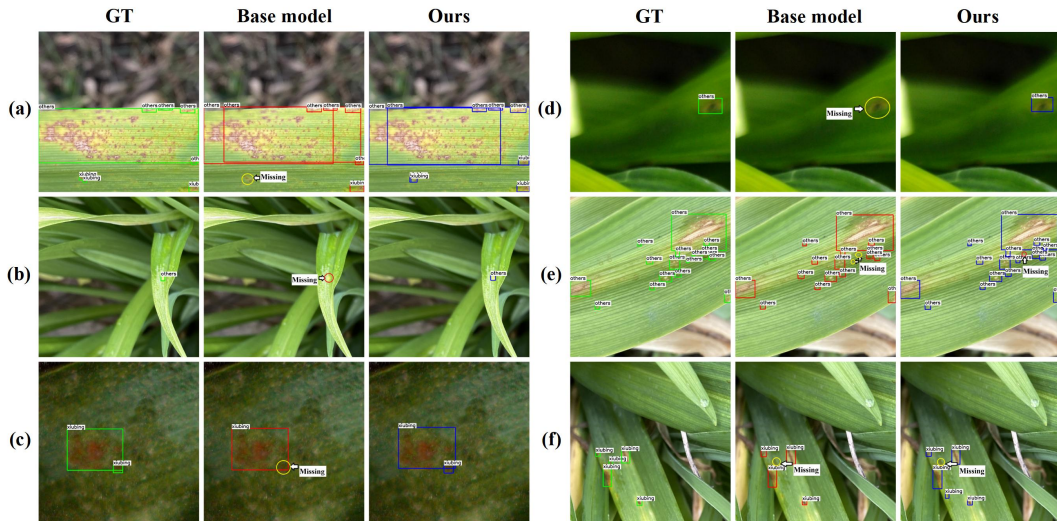


Fig. 13: Detection results: ours vs. base model.

Although YOLO12X achieves slightly higher recall, TCLeaf-Net provides a superior balance between precision and recall, as indicated by its leading F1 (60.8%). In addition, TCLeaf-Net attains these results with fewer parameters and lower computational cost compared to YOLO12X (46.1M vs. 59.1M parameters; 157.9 vs. 191.4 GFLOPs), further demonstrating its efficiency and practical value. These results highlight the effectiveness of TCLeaf-Net in challenging, real-world environments without reliance on large-scale pre-training.

Tomato-Leaf and Rice-Leaf. On the Tomato-Leaf dataset (Table 8 (left)), which contains relatively clean and controlled images, TCLeaf-Net attains the highest recall (88.8%) and mAP@50:95 (86.7%), while matching the best mAP@50 (94.6%). Its F1 (90.3%) also ranks highest, indicating robust performance even on simpler data. For the Rice-Leaf dataset (Table 8 (right)), which features lower image quality and increased visual noise, TCLeaf-Net again secures the best mAP@50 (57.3%) and mAP@50:95 (34.9%), as well as the top precision (67.8%) and a shared best F1 (59.9%).

Overall, TCLeaf-Net consistently achieves the best results or matches the best baseline across all three benchmarks, demonstrating strong cross-dataset generalization and resistance to overfitting. These findings confirm that the model's improvements are not confined to daylily imagery but generalize to diverse plant disease detection scenarios.

Table 7

Performance comparison on the PlantDoc dataset.

Model	PT	P(%) \uparrow	R(%) \uparrow	mAP@50(%) \uparrow	mAP@50:95(%) \uparrow	F1(%) \uparrow
YOLOv3(Shill and Rahman, 2021)	COCO	53.0	57.0	53.1	–	55.0
YOLOv4(Shill and Rahman, 2021)	COCO	53.0	62.0	55.5	–	56.0
NanoDet-Plus(Li et al., 2022b)	No M.	–	54.2	55.3	–	–
Improved-YOLOv5(Li et al., 2022b)	No M.	–	55.0	58.2	–	–
YOLOv8L(Moupojou et al., 2023)	COCO	–	–	55.0	–	–
YOLOv6L(Li et al., 2022a)	None	25.5	49.6	39.0	30.8	33.7
YOLOv9C(Zhang et al., 2024a)	None	57.4	58.9	60.9	47.9	58.1
YOLOv10L(Wang et al., 2024)	None	47.7	56.5	55.5	44.3	51.8
YOLO11L(Lee et al., 2024)	None	52.2	53.5	57.2	45.8	52.8
YOLO12L(Tian et al., 2025)	None	58.2	56.9	61.8	48.9	57.5
YOLO12X(Tian et al., 2025)	None	53.3	65.3	63.6	49.8	58.6
RTDETR-L(Zhao et al., 2023)	None	55.6	49.6	46.4	36.4	52.5
RTDETR-X(Zhao et al., 2023)	None	52.3	50.1	47.6	37.6	51.2
RTDETR-R50(Zhao et al., 2023)	None	53.2	54.6	50.6	40.1	53.9
RTDETR-R101(Zhao et al., 2023)	None	56.1	53.3	51.9	40.6	54.7
TCLLeaf-Net	None	59.4	62.2	65.7	52.5	60.8

Note. **PT:** Pretrained weights used. **No M.:** No mention. **COCO:** COCO pretrained. **None:** Trained from scratch. The symbol "–" indicates that the metric is not reported in the cited work.

Table 8

Comparison of model performance on Tomato-Leaf and Rice-Leaf datasets.

Model	Tomato-Leaf					Rice-Leaf				
	P(%) \uparrow	R(%) \uparrow	mAP@50(%) \uparrow	mAP@50:95(%) \uparrow	F1(%) \uparrow	P(%) \uparrow	R(%) \uparrow	mAP@50(%) \uparrow	mAP@50:95(%) \uparrow	F1(%) \uparrow
YOLOv3L	92.6	87.6	94.4	85.5	90.1	63.2	52.1	53.6	33.1	57.2
YOLOv5L	88.5	79.7	90.0	80.4	83.9	64.8	55.0	56.0	32.6	59.5
YOLOv6L	92.6	87.1	94.4	85.9	89.8	50.8	46.4	46.4	26.8	48.5
YOLOv8L	90.9	88.6	94.6	85.8	89.7	65.9	54.9	56.6	34.6	59.9
YOLOv9C	85.3	79.5	89.0	77.4	82.3	64.7	55.3	56.1	33.8	59.6
YOLOv10L	91.9	85.8	94.2	84.7	88.7	53.9	48.6	46.6	26.7	51.1
YOLO11L	91.0	88.7	94.6	85.8	89.9	60.2	52.6	54.0	33.3	56.2
YOLO12L	92.1	87.0	94.3	85.6	89.5	61.3	54.6	55.9	34.0	57.8
YOLO12X	91.9	87.9	94.3	85.3	89.8	61.9	54.5	57.0	34.3	58.0
RTDETR-L	87.5	80.8	88.5	78.6	84.0	52.1	50.0	46.3	28.8	51.1
RTDETR-X	87.2	80.8	88.5	78.9	83.9	55.0	44.7	44.8	27.8	49.3
RTDETR-R50	89.8	83.6	90.3	81.7	86.6	52.7	44.6	45.2	27.6	48.3
RTDETR-R101	88.7	84.0	90.4	81.9	86.3	55.3	47.1	47.0	28.1	50.9
TCLLeaf-Net	91.8	88.8	94.6	86.7	90.3	67.8	53.6	57.3	34.9	59.9

Note. All models trained from scratch.

4. Discussion

This study addresses two long-standing issues in plant-disease detection: (i) the scarcity of high-quality, field-collected public datasets and (ii) the poor robustness of existing detectors in complex outdoor scenes. We therefore publish two lesion-level, daylily leaf datasets and propose TCLLeaf-Net, a detector that remains reliable under real-world conditions. TCLLeaf-Net is built from three interchangeable blocks: TCM, RSFRS and DFPPN. These blocks are responsible for spatial modeling, semantic recovery and multi-scale fusion, respectively. This design is transferable to other crops.

Ablation studies (Table 3 (In-field dataset)) confirm that every block improves performance, with TCM contributing the largest single gain. RSFRS alone yields notable improvements, particularly on recall and overall mAP, and its combination with TCM produces a marked additional boost, indicating effective semantic recall. Adding DFPN further raises recall and F1, although a slight drop in mAP@50:95 on the in-field dataset reveals a minor trade-off in localization precision. Future work will tune deformable-convolution settings and cross-resolution fusion within DFPN to mitigate this effect.

To probe how TCLeaf-Net makes its decisions, we visualized Grad-CAM heatmaps (Selvaraju et al., 2017) generated by its three detection heads. The maps reveal which image regions influence each head and thus guide further design refinements.

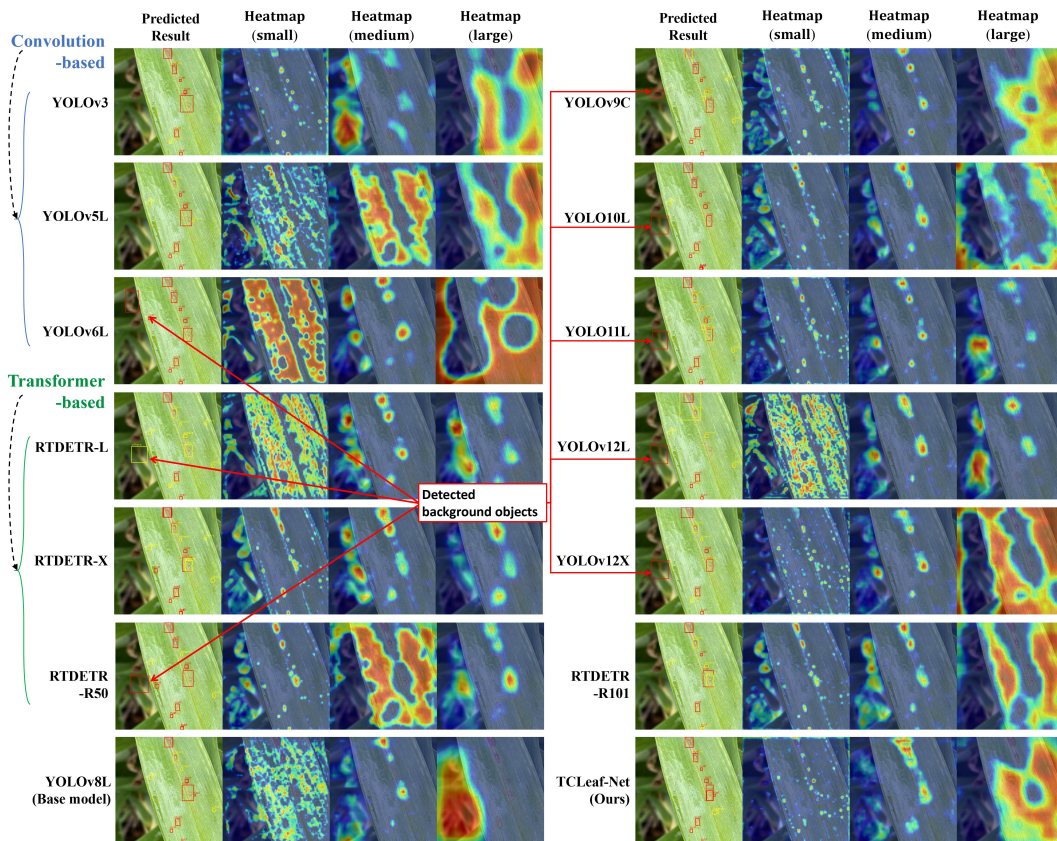


Fig. 14: Detection results and decision regions of different models.

Fig. 14 contrasts TCLeaf-Net with 13 representative baselines. TCLeaf-Net focuses on lesion pixels, accurately detecting them even when symptoms are very faint, while effectively suppressing background

clutter. By contrast, the baselines exhibit diffuse attention that often blankets whole leaves or the surrounding scene, leading to false activations.

This sharp focus stems mainly from the TCM: its three-branch TCL architecture fuses global and local cues, echoing earlier evidence in favor of hybrid attention (Liu et al., 2024; Ibtehaz et al., 2024). To quantify each branch’s contribution, we carried out additional ablations that track how branch removal alters the heatmaps and the final detection scores.

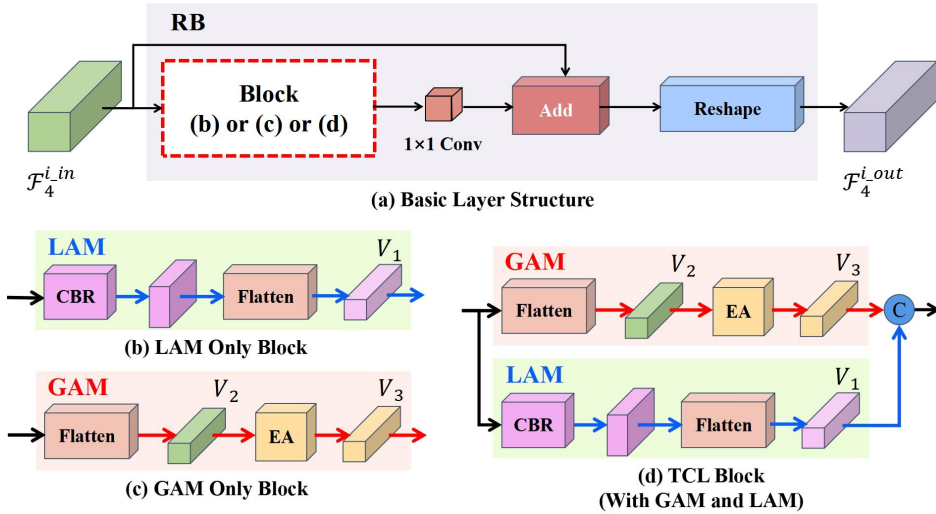


Fig. 15: Architectures used in the ablation study of different branches within TCL.

4.1. Effect of different branches of TCM

We performed ablation studies on three variants of the TCM: (b) LAM-only Block, which consists solely of the local attention branch (convolution) combined with a residual block (RB); (c) GAM-only Block, which contains only the global attention branch (transformer) with an RB; and (d) TCL Block (this work), which integrates both transformer and convolution branches along with an RB, as illustrated in Fig. 15(b)-(d). The basic layer structure is shown in Fig. 15(a), with (b), (c), and (d) corresponding to the LAM-only model, GAM-only model, and TCM.

To isolate the benefit of joint global-local processing, we built three variants of the TCM (Fig. 15(b)-(d)). LAM-only keeps just the local attention path (convolution) plus a residual block (RB); GAM-only keeps only the global attention path (transformer) and an RB; TCL integrates both paths and the RB.

Table 9

Ablation study on each branch of TCL on Daylily-Leaf (in-field) dataset.

Branch Scheme	P (%)	R (%)	mAP@50 (%)	mAP@50:95 (%)	F1 (%)
LAM-only	86.8	63.1	74.1	53.1	73.0
GAM-only	86.5	65.3	75.2	52.8	74.4
GAM+LAM (TCL)	87.2	69.9	78.2	55.1	77.6

Table 9 clearly demonstrates that TCL (GAM+LAM) achieves the highest recall (69.9%) among all models, indicating its superior ability to detect true positives in complex scenarios. In addition, TCL also delivers the best mAP@50 (78.2%) and F1 (77.6%), while maintaining a high precision (87.2%).

In comparison, LAM-only achieves the highest precision (86.8%) but suffers from a lower recall (63.1%), and GAM-only provides a moderate improvement in recall (65.3%) with slightly reduced precision (86.5%).

These results highlight that integrating local and global cues in TCL significantly boosts the detection rate without sacrificing overall accuracy.

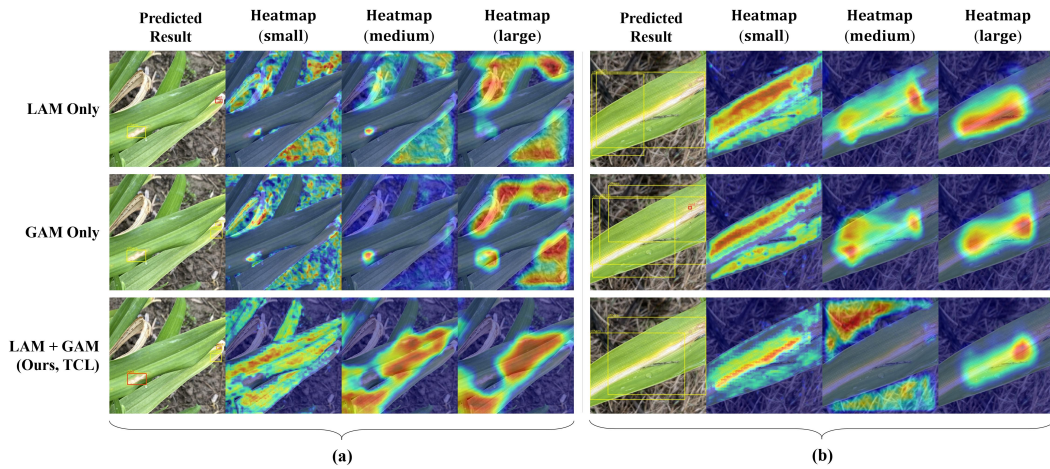


Fig. 16: Decision maps generated by GAM, LAM, and TCL for Example 1(a) and Example 2(b).

Grad-CAM heatmaps in Figs.16 and 17 reinforce the numbers. TCL focuses tightly on lesions, GAM-only spreads attention across whole leaves and textured backgrounds, and LAM-only splits focus between lesions and irrelevant pixels. For large lesions (Fig. 16(a)), TCL covers the symptomatic area most completely, though some lesions still extend beyond a single bounding box, suggesting room for hyper-parameter tuning.

As illustrated in Fig. 16(a) and Figs. 17(a)-17(b), the GAM-only model exhibits diffuse attention: its heatmaps spread beyond lesion regions, especially when (i) leaves occupy most of the frame (e.g., Fig. 17(a))

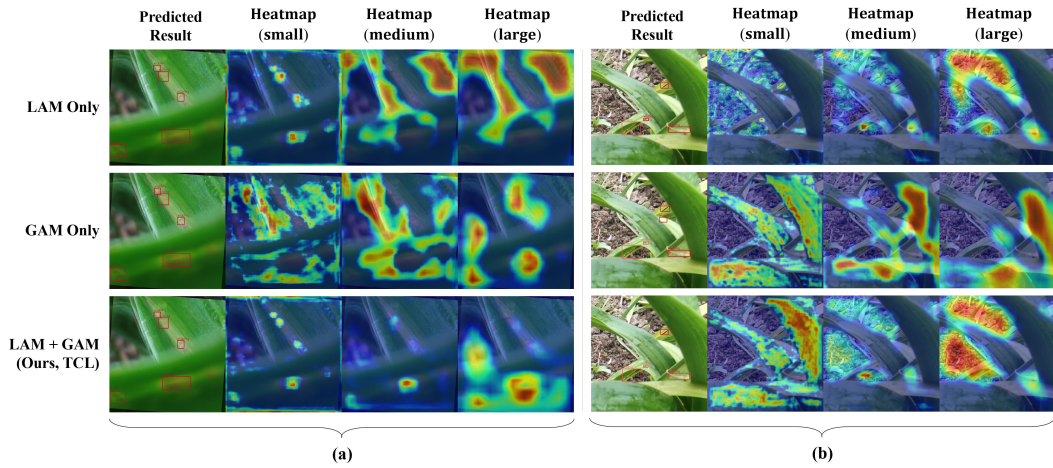


Fig. 17: Decision maps generated by GAM, LAM, and TCL for Example 3(a) and Example 4(b).

or (ii) the background contains rich texture (e.g., Figs. 16(a), 17(b)). In such cases the peak response drifts away from the lesion center, weakening the network’s ability to delineate boundaries and increasing the risk of missed detections. This behavior echoes previous observations of global-attention dispersion under clutter (Li et al., 2024).

Combining the LAM branch with the GAM branch restores spatial locality, constraining attention to lesion-relevant regions while complementing the global context modeling provided by GAM. The resulting TCL heatmaps remain lesion-centered and resist background interference, demonstrating stronger robustness under field conditions.

This suggests that controlling both the spatial extent and the central intensity of attention is crucial for reliable disease detection. Although TCLeaf-Net significantly improves attention focus and suppresses responses to background clutter, its attention intensity on lesion centers does not always surpass that of LAM-only in certain scenes, such as Fig. 17(a). Future work may focus on adaptive attention gating strategies to further enhance lesion-centered focus without compromising robustness.

In parallel with improving attention precision, computational efficiency is another key consideration in real-world deployments. Within TCM, the GAM branch accounts for most of the computational overhead, as global attention is commonly implemented using MHSA. To reduce resource consumption, we employ efficient attention (EA), which maintains global modeling capability with lower cost (Qin et al., 2023; Ma and Lan, 2024). Given EA’s central role in the GAM branch, we further investigate its standalone effectiveness below.

Table 10

Comparison of global attention mechanisms on the Daylily-Leaf (in-field) dataset.

Type	GPU (GB)↓	Time (h)↓	P (%)↑	R (%)↑	mAP@50 (%)↑	mAP@50:95 (%)↑	F1 (%)↑
MHSA*	~25.0	1.04	85.4	69.9	77.2	55.8	76.9
CA*	~26.1	1.06	87.3	67.3	78.0	56.8	76.0
EA	9.4	0.66	87.2	69.9	78.2	55.1	77.6

Note. **Type** = Attention mechanism; **GPU** = Memory usage during training (GB); **Time** = Total training time (hours);

* Due to out-of-memory (OOM) on the RTX 4090D (24GB), training was conducted on a 32GB GPU.

4.2. Effectiveness of efficient attention (EA)

To evaluate the role of EA in TCLeaf-Net, we replaced it with two commonly used global attention mechanisms: MHSA and cross-attention (CA). Table 10 summarizes the results.

EA achieves the highest mAP@50 and F1 among the three, while matching MHSA in recall and slightly surpassing it in precision. Compared to CA, which yields the best precision (87.3%), EA maintains nearly equivalent precision (87.2%) but gains a 2.6% recall advantage, leading to the best F1 (77.6%). This suggests that EA is more balanced, capturing additional true positives without significantly increasing false positives.

In terms of efficiency, EA requires only 9.4 GB of GPU memory-less than half of what MHSA and CA consume-and reduces total training time by over 37%. MHSA and CA also exhibit out-of-memory (OOM) issues on 24 GB cards in training, limiting their practicality for mid-range GPUs.

These results highlight EA's favorable trade-off between accuracy and efficiency. It supports effective global feature extraction under limited computational budgets, making TCLeaf-Net deployable on consumer-grade GPUs such as the RTX 3060 (12 GB), without compromising performance in complex agricultural scenarios.

Beyond controlled evaluations, field conditions present unpredictable challenges. We therefore examine TCLeaf-Net's robustness under various synthetic distortions.

4.3. Robustness of TCLeaf-Net against environmental variations

To test the TCLeaf-Net's real-world resilience, we generated three types of synthetic perturbations: rain streaks that emulate adverse weather, a compound rotation with channel shifts that reproduces camera shake, and low-light sensor noise typical of night-time photography. Figs. 18-19 show that TCLeaf-Net remains accurate under each condition, whereas the base model either misses lesions or misclassifies background regions.

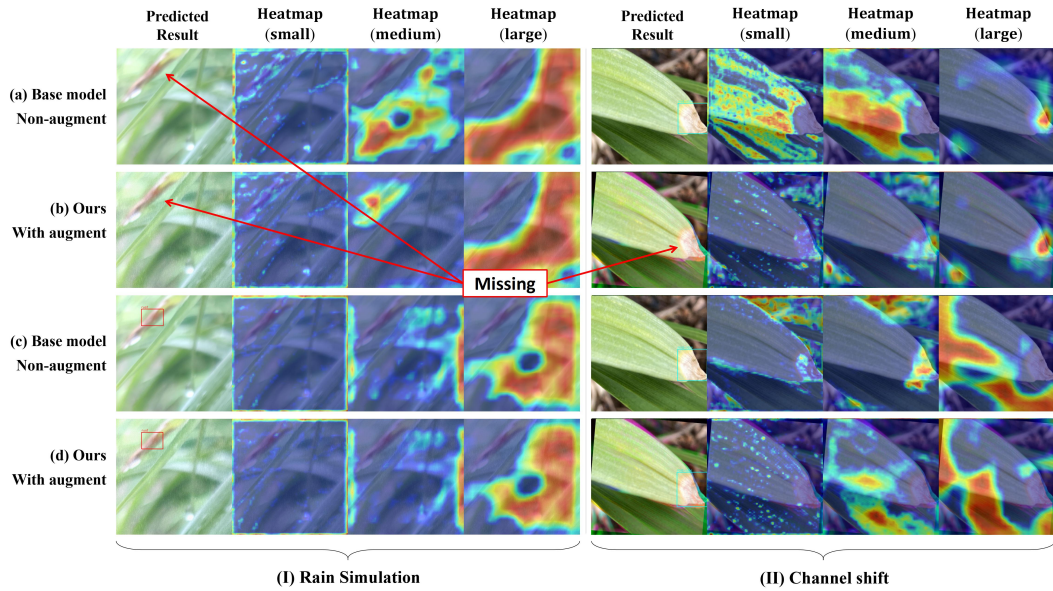


Fig. 18: Comparison of detection results and decision maps under (a) simulated rainy conditions and (b) simulated jitter, channel shift conditions.

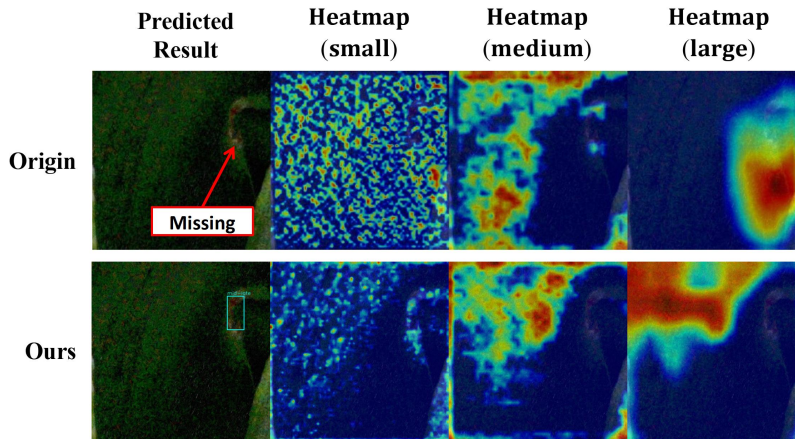


Fig. 19: Comparison of detection results and decision maps in low-light and noisy complex environments.

Under rainy condition (Fig. 18(a)), TCLeaf-Net still localizes the target, whereas the base model misses it entirely. After rotation and color shift (Fig. 18(b)) the baseline fails again, but TCLeaf-Net preserves tight boxes. In dim, noisy scenes (Fig. 19) TCLeaf-Net identifies lesions correctly, while the baseline misclassifies background patches. These examples underline the model's robustness to typical field-level distortions.

4.4. Limitations

While TCLeaf-Net demonstrates strong performance across multiple datasets and perturbation scenarios, several limitations remain that warrant further investigation.

First, although the transformer-convolution module (TCM) fuses global and local representations via 1×1 convolutions, the fusion weights are spatially uniform and shared across positions. This may limit the model's ability to dynamically adjust feature contributions across different lesion sizes or background conditions. In some cases, transformer-dominant responses may produce overly diffuse attention maps, while convolution-dominant responses may miss long-range dependencies.

Second, the current design of the multi-scale detection heads is strictly hierarchical: features from different levels are assigned to distinct heads without cross-level refinement. This structure can lead to fragmented predictions when lesions of different scales overlap or when small lesions appear near large ones. While DFPN improves alignment, its scale routing remains fixed. Introducing inter-head communication or scale-aware fusion may help address this issue.

Third, the Daylily-Leaf dataset, although annotated at lesion level and collected under diverse conditions, includes only one plant species and a limited number of symptom categories. This restricts the scope of generalization, especially for models intended for multi-crop deployment. Some complex or mixed symptoms are also coarsely labeled due to annotation constraints.

Future work will address these issues by incorporating spatially dynamic fusion in the backbone, refining cross-scale feature interactions, and expanding the dataset to include more crop species, a wider variety of disease symptoms, and different stages of plant growth with finer annotation granularity.

5. Conclusion

This study presents TCM-Net, a transformer-convolution hybrid architecture designed for robust lesion-level plant disease detection under complex in-field conditions. To support this objective, we construct Daylily-Leaf (ideal and in-field), a pair of lesion-level annotated datasets comprising fine-grained bounding boxes collected under both laboratory and real-world environments. Despite their compact scale, the datasets capture representative lesion patterns and background variability, providing a practical benchmark for instance-level plant disease detection in the wild.

Through extensive experiments, we observe that pure transformer-based detectors are prone to diffuse attention in cluttered backgrounds, likely due to their weak inductive biases and the lack of spatial priors. By integrating a convolutional branch, TCM-Net enhances spatial focus on leaf and lesion regions, effectively suppressing false positives arising from complex visual scenes.

In addition to its hybrid backbone, TCMLeaf-Net incorporates several architectural innovations to enhance feature representation and alignment. The SSOPE and RSFRS modules help preserve fine-grained spatial cues during early downsampling. The DFPN, equipped with multi-scale receptive fields and adaptive alignment, improves localization and semantic integration across scales.

On Daylily-Leaf, TCMLeaf-Net surpasses all 13 CNN- and transformer-based baselines, reaching $mAP@50 = 89.5\%/78.2\%$ (Ideal / In-Field) with 46.1 M parameters and 157.9 GFLOPs. On external leaf-level detection benchmarks (PlantDoc, Tomato-Leaf, Rice-Leaf), it attains $mAP@50 = 65.7\%, 94.6\%, 57.3\%$, respectively, demonstrating strong generalization and a practical computational footprint for deployment in diverse agricultural scenarios.

This study has two contributions:

- A small-scale yet carefully constructed lesion-level dataset, with rich annotations across varied lesion types and backgrounds, enabling fine-grained disease detection in real-world conditions;
- A hybrid detection framework that effectively addresses core limitations of existing CNN and transformer architectures under field conditions through improved feature preservation and robust background suppression.

These contributions lay the groundwork for further advancements in crop disease detection. Future work will focus on scaling the dataset to include more crop species and symptom types, optimizing model efficiency for mobile deployment, and exploring semi-supervised learning strategies to reduce annotation costs while maintaining lesion-level accuracy.

Declaration of competing interest

The authors declare that they have no known competing financial interests or personal relationships that could have appeared to influence the work reported in this paper.

Data availability

Data will be made available on reasonable request.

CRediT authorship contribution statement

Zishen Song: Conceptualization, Methodology, Software, Formal analysis, Writing - original draft, Writing - review & editing. **Yongjian Zhu:** Conceptualization, Methodology, Formal analysis, Writing - original draft, Funding acquisition, Writing - review & editing. **Dong Wang:** Project administration, Resources, Data curation, Writing - review & editing, Supervision. **Hongzhan Liu:** Resources, Funding acquisition, Supervision, Writing - review & editing. **Lingyu Jiang:** Validation, Formal analysis, Writing - review & editing. **Yongxing Duan:** Data curation, Writing - review & editing. **Zehua Zhang:** Investigation, Writing - review & editing. **Sihan Li:** Visualization, Writing - review & editing. **Jiarui Li:** Validation, Writing - review & editing.

References

- Attri, I., Awasthi, L.K., Sharma, T.P., Rathee, P., 2023. A review of deep learning techniques used in agriculture. *Ecological Informatics* 77, 102217.
- Banerjee, D., Kukreja, V., Gupta, A., Singh, V., Brar Tejinder, P.S., 2023. Combining cnn and svm for accurate identification of ridge gourd leaf diseases, in: *ASIANCON 2023 (IEEE Conference Proceedings)*, IEEE. pp. 1–5. Proposed hybrid CNN+SVM model for ridge gourd leaf disease identification.
- Bharathi, A.U.R., Seada, H., et al., 2025. Deep learning based ensemble model for accurate tomato leaf disease classification by leveraging resnet50 and mobilenetv2 architectures. *Scientific Reports* 15, 13904. doi:[10.1038/s41598-025-98015-x](https://doi.org/10.1038/s41598-025-98015-x).
- Bhargava, A., Shukla, A., Goswami, O.P., Alsharif, M.H., Uthansakul, P., Uthansakul, M., 2024. Plant leaf disease detection, classification, and diagnosis using computer vision and artificial intelligence: A review. *IEEE access* 12, 37443–37469.
- Chakrabarty, A., Ahmed, S.T., Islam, M.F.U., Aziz, S.M., Maidin, S.S., 2024. An interpretable fusion model integrating lightweight cnn and transformer architectures for rice leaf disease identification. *Ecological Informatics* 82, 102718.
- Choromanski, K., Likhoshesterov, V., Dohan, D., Song, X., Gane, A., Sarlos, T., Hawkins, P., Davis, J., Mohiuddin, A., Kaiser, L., et al., 2020. Rethinking attention with performers. *arXiv preprint arXiv:2009.14794*.
- Dong, J., Lee, J., Fuentes, A., Xu, M., Yoon, S., Lee, M.H., Park, D.S., 2022. Data-centric annotation analysis for plant disease detection: Strategy, consistency, and performance. *Frontiers in Plant Science* 13, 1037655. doi:[10.3389/fpls.2022.1037655](https://doi.org/10.3389/fpls.2022.1037655).
- Farjon, G., Liu, H., Edan, Y., 2023. Deep-learning-based counting methods, datasets, and applications in agriculture: a review. *Precision Agriculture* 24, 1683–1711. doi:[10.1007/s11119-023-10034-8](https://doi.org/10.1007/s11119-023-10034-8).
- Gao, S.H., Cheng, M.M., Zhao, K., Zhang, X.Y., Yang, M.H., Torr, P., 2019. Res2net: A new multi-scale backbone architecture. *IEEE transactions on pattern analysis and machine intelligence* 43, 652–662.
- Ghazal, S., Munir, A., Qureshi, W.S., 2024. Computer vision in smart agriculture and precision farming: Techniques and applications. *Artificial Intelligence in Agriculture*.
- Goyal, A., Bengio, Y., 2020. Inductive biases for deep learning of higher-level cognition. *arXiv preprint arXiv:2011.15091* URL: <https://arxiv.org/abs/2011.15091>. [Online; accessed 2025-07-11].
- Haikal, A.L.A., Yudistira, N., Ridok, A., 2024. Comprehensive mixed-based data augmentation for detection of rice leaf disease in the wild. *Crop Protection* 184, 106816.

Short Title of the Article

- Hossain, S., Mou, R.M., Hasan, M.M., Chakraborty, S., Razzak, M.A., 2018. Recognition and detection of tea leaf's diseases using support vector machine, in: 2018 IEEE 14th International Colloquium on Signal Processing & Its Applications (CSPA), IEEE, pp. 150–154.
- Huang, S., Lu, Z., Cheng, R., He, C., 2021. Fapn: Feature-aligned pyramid network for dense image prediction, in: Proceedings of the IEEE/CVF international conference on computer vision, pp. 864–873.
- Huang, X., Xu, D., Chen, Y., Zhang, Q., Feng, P., Ma, Y., Dong, Q., Yu, F., 2025. Econv-vit: A strongly generalized apple leaf disease classification model based on the fusion of convnext and transformer. *Information Processing in Agriculture*.
- Ibtehaz, N., Yan, N., Mortazavi, M., Kihara, D., 2024. Fusion of regional and sparse attention in vision transformers. *arXiv preprint arXiv:2406.08859* doi:[10.48550/arXiv.2406.08859](https://doi.org/10.48550/arXiv.2406.08859).
- Jafar, A., Bibi, N., Naqvi, R.A., Sadeghi-Niaraki, A., Jeong, D., 2024. Revolutionizing agriculture with artificial intelligence: plant disease detection methods, applications, and their limitations. *Frontiers in Plant Science* 15, 1356260.
- Ji, Y., Zhang, R., Wang, H., Li, Z., Wu, L., Zhang, S., Luo, P., 2021. Multi-compound transformer for accurate biomedical image segmentation, in: Medical Image Computing and Computer Assisted Intervention–MICCAI 2021: 24th International Conference, Strasbourg, France, September 27–October 1, 2021, Proceedings, Part I 24, Springer, pp. 326–336.
- Joher, G., Team, U., 2020. Yolov5. GitHub repository, <https://github.com/ultralytics/yolov5>.
- Joshi, K., Awale, R., Ahmad, S., Patil, S., Pisal, V., 2022. Plant leaf disease detection using computer vision techniques and machine learning, in: ITM Web of Conferences, EDP Sciences. p. 03002.
- Khan, R., Ud Din, N., Zaman, A., Huang, B., 2024. Automated tomato leaf disease detection using image processing: An svm-based approach with glcm and sift features. *Journal of Engineering* 2024, 9918296.
- Lee, Y.H., Zhang, C.Y., Wang, C.Y., Liao, H.Y.M., 2024. Yolov11: An overview of the key architectural enhancements. *arXiv preprint arXiv:2410.17725* doi:[10.48550/arXiv.2410.17725](https://doi.org/10.48550/arXiv.2410.17725).
- Li, B., Zhou, R., Yang, L., Wang, Q., Chen, H., 2024. Mildetr: detection transformer for military camouflaged target detection. *IEEE Access* 12, 26163–26174.
- Li, C., Ge, Z., Liu, C., et al., 2022a. Yolov6: A single-stage object detection framework for industrial applications. *arXiv preprint arXiv:2209.02976*.
- Li, D., Li, L., Chen, Z., Li, J., 2025. Shiftwiseconv: Small convolutional kernel with large kernel effect, in: Proceedings of the Computer Vision and Pattern Recognition Conference, pp. 25281–25291.
- Li, J., Qiao, Y., Liu, S., Zhang, J., Yang, Z., Wang, M., 2022b. An improved yolov5-based vegetable disease detection method. *Computers and Electronics in Agriculture* 202, 107345.
- Lin, T.Y., Dollár, P., Girshick, R., He, K., Hariharan, B., Belongie, S., 2017. Feature pyramid networks for object detection, in: Proceedings of the IEEE Conference on Computer Vision and Pattern Recognition (CVPR), pp. 2117–2125. doi:[10.1109/CVPR.2017.106](https://doi.org/10.1109/CVPR.2017.106).
- Liu, D., Liang, J., Geng, T., Loui, A., Zhou, T., 2023. Tripartite feature enhanced pyramid network for dense prediction. *IEEE Transactions on Image Processing* 32, 2678–2692.
- Liu, J., Wang, X., Chen, Q., Yan, P., Liu, X., 2025. Deep learning method for cucumber disease detection in complex environments for new agricultural productivity. *BMC Plant Biology* 25, 888.
- Liu, S., Huang, D., et al., 2018. Receptive field block net for accurate and fast object detection, in: Proceedings of the European conference on computer vision (ECCV), pp. 385–400.
- Liu, Y., Wu, Y.H., Sun, G., Zhang, L., Chhatkuli, A., Van Gool, L., 2024. Vision transformers with hierarchical attention. *Machine Intelligence Research* 21, 670–683. doi:[10.1007/s11633-024-1393-8](https://doi.org/10.1007/s11633-024-1393-8).

- Ma, Y., Lan, X., 2024. Semantic segmentation using cross-stage feature reweighting and efficient self-attention. *Image and Vision Computing* 145, 104996.
- Mingyue, S., Jianhua, Z., Quan, F., Xiujuan, C., Ning, Z., Wenrong, Z., 2022. Research progress of deep learning in detection and recognition of plant leaf diseases. *Smart Agriculture* 4, 29. doi:[10.12133/j.smartag.SA202202005](https://doi.org/10.12133/j.smartag.SA202202005).
- Moupojou, E., Tagne, A., Retraint, F., Tadonkemwa, A., Wilfried, D., Tapamo, H., Nkenlifack, M., 2023. Fieldplant: A dataset of field plant images for plant disease detection and classification with deep learning. *IEEE Access* 11, 35398–35410.
- Peng, J., Li, S., Ma, X., Ding, H., Fang, W., Bi, R., 2024. Spatial distribution and influencing factors of daylily cultivation in the farming–pastoral ecotone of northern china. *Land* 13. doi:[10.3390/land13040439](https://doi.org/10.3390/land13040439).
- Qin, H., Zhou, D., Xu, T., Bian, Z., Li, J., 2023. Factorization vision transformer: Modeling long-range dependency with local window cost. *IEEE Transactions on Neural Networks and Learning Systems* .
- Redmon, J., Farhadi, A., 2018. Yolov3: An incremental improvement. *arXiv preprint arXiv:1804.02767* .
- Reis, H.C., Turk, V., 2024. Potato leaf disease detection with a novel deep learning model based on depthwise separable convolution and transformer networks. *Engineering Applications of Artificial Intelligence* 133, 108307.
- Ristaino, J.B., Anderson, P.K., Bebb, D.P., Brauman, K.A., Cunniffe, N.J., Fedoroff, N.V., Finegold, C., Garrett, K.A., Gilligan, C.A., Jones, C.M., et al., 2021. The persistent threat of emerging plant disease pandemics to global food security. *Proceedings of the National Academy of Sciences* 118, e2022239118.
- Sagar, N., Suresh, K.P., Sridhara, S., Patil, B., Archana, C.A., Sekar, Y.S., Naveesh, Y.B., Nandan, A.S., Sushma, R., 2025. Precision detection of grapevine downy and powdery mildew diseased leaves and fruits using enhanced resnet50 with batch normalization. *Computers and Electronics in Agriculture* 232, 110144.
- Selvaraju, R.R., Cogswell, M., Das, A., Vedantam, R., Parikh, D., Batra, D., 2017. Grad-cam: Visual explanations from deep networks via gradient-based localization, in: *Proceedings of the IEEE international conference on computer vision*, pp. 618–626.
- Shill, A., Rahman, M.A., 2021. Plant disease detection based on yolov3 and yolov4, in: *2021 International Conference on Automation, Control and Mechatronics for Industry 4.0 (ACMI)*, IEEE. pp. 1–6.
- Shu, Y., Bain, M.E., 2024. Retina vision transformer (retinavit): Introducing scaled patches into vision transformers. *arXiv preprint arXiv:2403.13677* .
- Simhadri, C.G., Kondaveeti, H.K., Vatsavayi, V.K., Mitra, A., Ananthachari, P., 2024. Deep learning for rice leaf disease detection: A systematic literature review on emerging trends, methodologies and techniques. *Information Processing in Agriculture* .
- Szegedy, C., Liu, W., Jia, Y., Sermanet, P., Reed, S., Anguelov, D., Erhan, D., Vanhoucke, V., Rabinovich, A., 2015. Going deeper with convolutions, in: *Proceedings of the IEEE conference on computer vision and pattern recognition*, pp. 1–9.
- Team, U., 2023. Yolov8. *GitHub repository*, url<https://github.com/ultralytics/ultralytics>.
- Thai, H.T., Le, K.H., 2025. Mobileh-transformer: Enabling real-time leaf disease detection using hybrid deep learning approach for smart agriculture. *Crop Protection* 189, 107002. doi:[10.1016/j.cropro.2024.107002](https://doi.org/10.1016/j.cropro.2024.107002).
- Thai, H.T., Le, K.H., Nguyen, N.L.T., 2023. Formerleaf: An efficient vision transformer for cassava leaf disease detection. *Computers and Electronics in Agriculture* 204, 107518.
- Tian, Y., Ye, Q., Doermann, D., 2025. Yolov12: Attention-centric real-time object detectors. *arXiv preprint arXiv:2502.12524* .
- Tiancan, J., et al., 2024. Identification of tomato leaf diseases based on dgp-snnnet. *Crop Protection DGP-SNNet with PConv and two-stage transfer learning achieved 99.55 percent accuracy on tomato leaves*.
- Touvron, H., Cord, M., El-Nouby, A., Verbeek, J., Jégou, H., 2022. Three things everyone should know about vision transformers, in: *European Conference on Computer Vision*, Springer. pp. 497–515.

Short Title of the Article

- Ullah, N., Khan, J.A., Almakdi, S., Alshehri, M.S., Al Qathrady, M., El-Rashidy, N., El-Sappagh, S., Ali, F., 2023. An effective approach for plant leaf diseases classification based on a novel deeplantnet deep learning model. *Frontiers in Plant Science* Lightweight 28-layer DeepPlantNet achieves 99% accuracy on 10 disease classes.
- Valanarasu, J.M.J., Oza, P., Hacıhaliloglu, I., Patel, V.M., 2021. Medical transformer: Gated axial-attention for medical image segmentation, in: de Bruijne, M., Cattin, P.C., Cotin, S., Padoy, N., Speidel, S., Zheng, Y., Essert, C. (Eds.), *Medical Image Computing and Computer Assisted Intervention – MICCAI 2021*, Springer International Publishing, Cham. pp. 36–46.
- Van Quyen, T., Kim, M.Y., 2023. Feature pyramid network with multi-scale prediction fusion for real-time semantic segmentation. *Neurocomputing* 519, 104–113.
- Wang, A., Chen, H., Liu, L., et al., 2024. Yolov10: Real-time end-to-end object detection. *arXiv preprint arXiv:2405.14458* doi:[10.48550/arXiv.2405.14458](https://doi.org/10.48550/arXiv.2405.14458).
- Wang, K., Liew, J.H., Zou, Y., Zhou, D., Feng, J., 2019. Panet: Few-shot image semantic segmentation with prototype alignment, in: *proceedings of the IEEE/CVF international conference on computer vision*, pp. 9197–9206.
- Wei, W., Yue, H., Nie, Y., Chen, T., 2022. First report of colletotrichum siamense causing daylily (hemerocallis citrina) anthracnose in china. *Plant Disease* 106, 1061.
- Xu, X., Yang, G., Wang, Y., Shang, Y., Hua, Z., Wang, Z., Song, H., 2024. Plant leaf disease identification by parameter-efficient transformer with adapter. *Engineering Applications of Artificial Intelligence* 138, 109466.
- Zhang, C.Y., Wang, C.Y., Liao, H.Y.M., 2024a. Yolov9: Learning what you want to learn using programmable gradient information. *arXiv preprint arXiv:2402.13616* doi:[10.48550/arXiv.2402.13616](https://doi.org/10.48550/arXiv.2402.13616).
- Zhang, S., Chi, C., Yao, Y., Lei, Z., Li, S.Z., 2020. Bridging the gap between anchor-based and anchor-free detection via adaptive training sample selection, in: *Proceedings of the IEEE/CVF conference on computer vision and pattern recognition*, pp. 9759–9768.
- Zhang, S., Chi, C., Yao, Y., Lei, Z., Li, S.Z., 2024b. Neural network based on convolution and self-attention fusion mechanism for plant leaves disease recognition. *Computers and Electronics in Agriculture* 202, 107002. doi:[10.1016/j.compag.2024.107002](https://doi.org/10.1016/j.compag.2024.107002).
- Zhang, S., Chi, C., Yao, Y., Lei, Z., Li, S.Z., 2024c. Potato leaf disease detection with a novel deep learning model based on depthwise separable convolution and transformer networks. *Computers in Biology and Medicine* 155, 106816. doi:[10.1016/j.combiomed.2024.106816](https://doi.org/10.1016/j.combiomed.2024.106816).
- Zhang, T., Xu, W., Luo, B., Wang, G., 2025. Depth-wise convolutions in vision transformers for efficient training on small datasets. *Neurocomputing* 617, 128998.
- Zhao, Y., Lv, W., Xu, S., Wei, J., Wang, G., Dang, Q., Liu, Y., Chen, J., 2023. Detsr beat yolos on real-time object detection. *arXiv:2304.08069*.